



HAL
open science

On the use of a multi-site ion-exchange model to predictively simulate the adsorption behaviour of strontium and caesium onto French agricultural soils

Brice Siroux, Christelle Latrille, Catherine Beaucaire, Cristina Petcut, Michel Tabarant, Marc F. Benedetti, Pascal E. Reiller

► To cite this version:

Brice Siroux, Christelle Latrille, Catherine Beaucaire, Cristina Petcut, Michel Tabarant, et al.. On the use of a multi-site ion-exchange model to predictively simulate the adsorption behaviour of strontium and caesium onto French agricultural soils. *Applied Geochemistry*, 2021, 132, pp.105052. 10.1016/j.apgeochem.2021.105052 . cea-03309418

HAL Id: cea-03309418

<https://cea.hal.science/cea-03309418>

Submitted on 30 Jul 2021

HAL is a multi-disciplinary open access archive for the deposit and dissemination of scientific research documents, whether they are published or not. The documents may come from teaching and research institutions in France or abroad, or from public or private research centers.

L'archive ouverte pluridisciplinaire **HAL**, est destinée au dépôt et à la diffusion de documents scientifiques de niveau recherche, publiés ou non, émanant des établissements d'enseignement et de recherche français ou étrangers, des laboratoires publics ou privés.

On the Use of a Multi-Site Ion-Exchange Model to Predictively Simulate the Adsorption Behaviour of Strontium and Caesium Onto French Agricultural Soils

Brice Siroux,^a Christelle Latrille,^b Catherine Beaucaire,^b Cristina Petcut,^b Michel Tabarant,^a Marc F. Benedetti,^c Pascal E. Reiller^{a,*}

^a *Université Paris-Saclay, CEA, Service d'Études Analytiques et de Réactivité des Surfaces (SEARS), F-91191 Gif-sur-Yvette, France*

^b *Université Paris-Saclay, CEA, Service d'Études du Comportement des Radionucléides (SECR), F-91191 Gif-sur-Yvette, France*

^c *Université de Paris, Institut de Physique du Globe de Paris, CNRS, UMR 7154 CNRS, F-75238 Paris, France*

* *corresponding author: pascal.reiller@cea.fr*

ABSTRACT

In case of nuclear accident, ^{90}Sr and $^{134,137}\text{Cs}$ are major radionuclides to account. In previous works ([Appl. Geochem. 87, 167](#); [ibid 93, 167](#)), a database of ion-exchange parameters allowing the description of the Sr^{2+} and Cs^+ adsorption on purified illite and smectite was developed for a multi-site ion-exchange (MSIE) model. In this study, the adsorption behaviours of Sr^{2+} and Cs^+ were obtained with $<150\ \mu\text{m}$ fractions of French soil samples: a cambisol fluvic, a calcosol, and a cambisol typic. The $<2\ \mu\text{m}$ fractions of the soil samples were analysed by X-ray diffraction to estimate their clay minerals proportions that were then approximated to an illite/smectite mixture, in consistency with the CEC of the $<150\ \mu\text{m}$ fractions. The database was implemented with K-illite and -smectite parameters to account for the amendment of K^+ in agricultural soils. The isotherms of Sr^{2+} and Cs^+ on the three soils — at $0.033\ \text{mol kg}_w^{-1}\ \text{CaCl}_2$ ($I = 0.1\ \text{mol kg}_w^{-1}$) and at the pH value of the water equilibrated with the soils — were then compared with simulations obtained using ion-exchange parameters from the database for the MSIE model. This simulation approach, based on the additive adsorption properties between several

reactive phases, allowed to describe satisfactorily the adsorption of Sr^{2+} and Cs^+ in most cases. In order to highlight the limiting parameters of the modelling predictive ability, different treatments were made on soil samples. The removal of the natural organic matter did not change significantly the adsorption behaviour of either Sr^{2+} or Cs^+ . The removal of the exchangeable aluminium from the cambisol typic allowed a better simulation of the adsorption isotherm in the case of Sr^{2+} . Finally, in the case of the calcosol, the satisfactory modelling of the decrease in adsorption of Sr and Cs using a synthetic CaCl_2 pore water with increasing concentrations of KNO_3 allowed to verify the robustness of the MSIE model and exchange parameters from the database.

1 INTRODUCTION

Nuclear accident at the Fukushima-Daiichi Power Plant, after the Great Tohoku earthquake and tsunami on 11 March 2011 ([Hayes et al., 2017](#)), led to the release of a significant amount of radionuclides in the surrounding environment, out of which ^{137}Cs and ^{90}Sr , two main daughters of the fission of ^{235}U ([England and Rider, 1993](#)), were identified as major contaminants ([Kanda, 2013](#); [Kurokawa et al., 2020](#); [Sahoo et al., 2016](#); [Steinhauser et al., 2014](#); [Tanaka et al., 2012](#)). In order to understand the aftermath of this event, but also of the Chernobyl accident in 1986 ([Steinhauser et al., 2014](#)), and of global nuclear fallout ([Fujikawa et al., 1999](#); [Larionova et al., 2021](#); [Snyder et al., 2012](#)), the scientific community has enhanced the knowledge of the impact and mobility of the two radionuclides in the environment ([Bunzl et al., 1998](#); [Durrant et al., 2018](#); [Fujikawa et al., 1999](#); [Hou et al., 2003](#); [Matsunaga et al., 1998](#)). In France, 18 nuclear power plants (58 reactors) are currently in operation and provide more than 60% of the produced electricity (<https://www.rte-france.com/>). Therefore, the knowledge of the possible consequences due to a comparable accident is crucial.

^{90}Sr and ^{137}Cs are well known to have a low mobility in soils ([Han et al., 2016](#); [Mishra et al., 2016](#)) due to their strong interactions with clay minerals ([Adeleye et al., 1994](#); [Baborova et al., 2018](#); [Durrant et al., 2018](#); [Dyer et al., 2000](#); [Sawhney, 1970](#); [Semenkova et al., 2018](#)), out of which illite and vermiculite are known to be the most selective adsorbents for Cs^+ ([Durrant et al., 2018](#); [Dzene et al., 2015](#)). This high adsorption is due to the weak hydration energy of Cs^+ ([Marcus, 1985](#)) and mainly attributed to the existence of low concentration high affinity sites, usually referred as frayed edge sites (FES) on illite ([Cornell, 1993](#); [Sawhney, 1972](#)). Sr^{2+} is also significantly retained by clay minerals but has a lower affinity for specific high affinity sites ([Erten et al., 1988](#); [Galamboš et al., 2013](#); [Missana et al., 2008](#); [Siroux et al., 2017a](#); [Siroux et al., 2018](#); [Wissocq et al., 2018](#)).

In soils, natural organic matter (NOM) also influences the adsorption of Cs^+ . The specific interaction of Cs^+ with humic substances, extracted from NOM, is weak and comparable to, even slightly lower than, the interaction of other alkaline metals, also due to the weak and chaotropic hydration of Cs^+ ([d'Orlyé and Reiller, 2012](#)). It was evidenced that the NOM coating of clay minerals tends to decrease the adsorption of Cs^+ ([Dumat et al., 2000](#); [Tashiro et al., 2018](#)). The removal of the initial NOM from soils also seemed to enhance the adsorption of Cs^+ ([Dumat et al., 1997](#)); these effects were more important at low concentration of Cs ([Dumat and Staunton, 1999](#)). [Staunton et al. \(2002\)](#) proposed that NOM was fixed on the anion-exchange sites, mainly at the particle edges and close to the FES, physically blocking the access to the adsorption sites for Cs^+ . The effects of NOM on the adsorption of Sr^{2+} onto soils were scarcely studied. [Samadfam et al. \(2000\)](#) have only evidenced a slight reduction of the adsorption of Sr^{2+} onto a kaolinite after addition of humic acid.

The adsorption of Sr^{2+} and Cs^+ onto soils has been commonly interpreted with semi-empirical approaches as the Langmuir or the Freundlich isotherms ([Campbell and Davies, 1995](#); [Goto et al., 2008](#); [Gutierrez and Fuentes, 1991](#)). These approaches only permit a description of the

adsorption under fixed physicochemical conditions, which prevent from extrapolating results to other conditions. Different thermodynamic models, as surface complexation ([Dzombak and Morel, 1990](#); [Karamalidis and Dzombak, 2010](#); [Tournassat et al., 2018](#)), and ionic exchange modelling ([Gaines and Thomas, 1953](#); [Tournassat et al., 2009](#)), have been proposed to improve the knowledge and the description of the adsorption phenomena. Out of these thermodynamic modelling, the multi-site ion-exchange (MSIE) model has been successfully used to interpret the adsorption behaviour of multiple cations in various clays minerals and sediments ([Jacquier et al., 2004](#); [Motellier et al., 2003](#); [Reinoso-Maset and Ly, 2014](#); [Savoie et al., 2015](#); [Siroux et al., 2017a](#); [Siroux et al., 2018](#); [Stammose et al., 1992](#); [Tertre et al., 2009](#); [Wissocq et al., 2018](#)). This model is designed to describe the adsorption at a macroscopic scale, and allows accounting both for the competition between ions for adsorption sites and for the solution chemistry of the elements — e.g, complexation and hydrolysis. By applying the MSIE model, it is possible to describe an exchanger in two ways: (i) as a unique and specific phase; and (ii) through an additive approach. [Motellier et al. \(2003\)](#) characterised directly the Callovo-Oxfordian claystone in terms of site capacities and corrected selectivity coefficients of adsorbed species activities with the MSIE modelling. [Tertre et al. \(2009\)](#) also used this principle for Zn mobility in clayey sediments by considering clay minerals (*i.e.*, soil and sediment) chemical reactivity to the one of pure montmorillonite. Conversely, the additivity approach permits extrapolating the modelling to various types of materials according to their clay minerals compositions — see *e.g.* [Durrant et al. \(2018\)](#) and [Siroux et al. \(2018\)](#).

In this study, the predictive character of the modelling approach is based on the additivity of the adsorption properties of reactive phases acting in the studied media. This method consists in: (i) determining and quantifying the clay mineral proportions (compositions and amounts) from soil samples; (ii) approximating the clay mineral proportions to an illite/smectite mixture in agreement with the original characteristics of soils (mineralogical composition, CEC); and

(iii) applying the model to simulate the adsorption of Cs^+ and Sr^{2+} onto these soils. [Savoye et al. \(2012\)](#) and [Wissocq et al. \(2018\)](#) used this principle to study the Cs mobility through the Callovo-Oxfordian claystone and a clayey sandstone, respectively. [Missana et al. \(2014\)](#), using the [Gaines and Thomas \(1953\)](#) formalism of the ion-exchange, have represented the adsorption of Cs^+ on various soils and sediments according to their illite, smectite, and kaolinite compositions. [Zavarin et al. \(2005\)](#) used an approach comparable to MSIE and showed the predominance of illite adsorption properties for Cs compared to kaolinite and smectite (montmorillonite). It can be noted that the equivalent H^+/Na^+ exchange reactions on clays were not accounted for in [Durrant et al. \(2018\)](#), when it was for calcite in [Zavarin et al. \(2005\)](#).

In France, the most common clay minerals encountered in soils are dominantly smectite, illite, and kaolinite, and in a minor extent chlorite and vermiculite. Smectite and illite adsorption properties have been recently studied applying the MSIE modelling by [Siroux et al. \(2017a\)](#), [Siroux et al. \(2018\)](#), and [Wissocq et al. \(2018\)](#). The additive approach was tested by [Siroux et al. \(2018\)](#) and [Wissocq et al. \(2018\)](#). [Reinoso-Maset and Ly \(2014\)](#) explored the exchange properties of kaolinite (Na^+/H^+ , K^+/H^+ , Cs^+/H^+ , $\text{Ca}^{2+}/\text{H}^+$, $\text{Mg}^{2+}/\text{H}^+$, Cl^-/OH^- , and $\text{ClO}_4^-/\text{OH}^-$), but the behaviour of Sr^{2+} was not included in the study. [Ning et al. \(2017\)](#) evidenced only one type of site for the Sr^{2+} adsorption on an Na-kaolinite. Studies are missing in the literature concerning chlorite.

The objective of this work is to provide an applicative and operational model capable to predict the adsorption of Sr and Cs onto agricultural French soils, and give relevant information on the mobility of these elements for the decision-making authorities. Knowing the complexity of a soil, some assumptions must be made in order to consider first order phenomena. In this study, the modelling through the additivity approach was examined to predict the adsorption of Cs^+ and Sr^{2+} onto three French agricultural soil samples. First, each soil sample was examined in terms of the major clay minerals compositions, i.e., illite/smectite or illite/smectite/kaolinite.

Adsorption isotherms of Cs⁺ and Sr²⁺ were acquired in a large range of concentration on these soil samples, and at the pH values measured for each soil equilibrated with pure water (pH_{water}), and considering Ca²⁺ as the major cation in the equilibrium solution. The experimental partition coefficients (R_D) were compared to the ones obtained from simulations using MSIE modelling. In order to improve these simulations the influence of NOM and exchangeable Al on the adsorption was explored. The possible improvement on the simulations of the account of kaolinite was also studied. Finally, the predictive capacity of the modelling was tested in simplified synthetic waters that can be representative of a potassium-amended soil pore water.

2 MATERIALS AND METHODS

2.1 Soils samples

2.1.1 Sampling

Three French agricultural soil samples were collected near Pusignan (Rhône, F-69330) and Étoile-sur-Rhône (Drôme, F-26800) from fields managed by ARVALIS (<https://www.arvalis-infos.fr>), and near Herqueville (Manche, F-50440) from a field managed by ORANO (formerly Areva, <https://www.orano.group/en/orano-home>). These soils were selected for their representative character of the agricultural soil diversity surrounding the French nuclear sites. These soils are classified as cambisol fluvic (Pusignan), cambisol typic (Herqueville), and calcosol (Étoile-sur-Rhône) according to the FAO nomenclature. The topsoil A horizon was collected after removal of vegetation, air dried, and sieved at 2 mm.

2.1.2 Preparation

To avoid both coarse sand and gravels, and to optimize the soil aliquots homogeneity, the less than 2 mm dry soil was dry-sieved at 150 µm. First, experiments were made with these untreated materials. For experiments on soils without NOM, soils samples were placed in H₂O₂

15% and heated at 80°C under agitation until the mixtures stop bubbling. Samples were washed first with Milli-Q water (Millipore, 18.2 MΩ cm⁻¹), then with ethanol. This operation was repeated twice, then the organic carbon and nitrogen contents were analysed in an automatic CHNS analyser (Thermofisher) after acidification of samples with 8% H₃PO₄. The removing of dissolved Al in the cambisol typic was performed with several washings with 1 mol kg_w⁻¹ KCl solution at pH value ca. 4. The extraction of dissolved Al was followed measuring the concentrations of Al and Si in supernatants. Finally, the soils were rinsed with 0.1 mol kg_w⁻¹ CaCl₂, then with ethanol.

2.1.3 Characterization

Grain-size fractionations were performed on untreated 2 mm soil samples by wet sieving and sedimentation following the AFNOR NF X31-107 standard. Soil samples were divided into five grain-size fractions: coarse sand (>200 μm), fine sand (200-50 μm), coarse silt (50-20 μm), fine silt (20-2 μm), and clay (<2 μm).

The organic matter (OM) was determined by the volatile loss at 550°C. The CaCO₃ concentration was measured following the Bernard calcimetre method (AFNOR NF ISO 10693), and the pH_{water} and pH_{KCl} measurements were performed following the standard French procedure NF ISO 10390.

The cation-exchange capacities (CEC) and the exchangeable cations (Ca²⁺, Na⁺, K⁺, and Mg²⁺) concentrations of the three soils were determined on the <2 mm soils by using the Metson method (NF X31-130), and on the less than 150 μm soil sample by K⁺/Cs⁺ exchange. Then, the CEC was measured by extracting all exchangeable cations with a 0.1 mol kg_w⁻¹ KCl solution at pH value ca. 10 (KOH) during one day to replace them by K⁺. Supernatant was removed and the soil was washed with Milli-Q water, then with ethanol. The adsorbed K⁺ was extracted with a 0.1 mol kg_w⁻¹ CsCl solution, and analysed by ICP-AES. To determine the exchangeable cations

concentrations, soil samples were put in contact with a $0.1 \text{ mol kg}_w^{-1}$ CsCl solution during 3 days, then supernatants were removed and analysed by ICP-AES.

The CEC of the three soils was also determined on $<2 \text{ }\mu\text{m}$ soil fractions obtained by grain-size fraction of the bulk soils ($<2 \text{ mm}$). After a H_2O_2 treatment, CEC was measured with the MgCl_2 method ([Righi et al., 1993](#)). It consists in saturating samples with MgCl_2 , the excess of which is removed with ethanol. Finally, Mg^{2+} are exchanged with NH_4^+ and measured by atomic absorption spectroscopy.

The mineralogical composition was estimated by X-ray Diffraction on untreated 2 mm soil samples reduced in powder and on clay fractions prepared as air-dried deposits and deposits saturated with ethylene glycol. The soils heated to 105 and 500°C were analysed by XRD. These treatments were performed in order to refine the mineralogical analysis. Identification of crystallized phases used the ClayXR software ([Bouchet, 1992](#)) and NEWMOD software ([Reynolds, 1985](#)) for quantification. Quantification of the clay minerals in soils is based on the quantification of clay minerals contained in the clay size-fraction ($<2 \text{ }\mu\text{m}$) of soils after OM removal.

2.2 Adsorption isotherm experiments

2.2.1 Chemicals reagents

The chemicals reagents used were of analytical grade or higher. Stable Sr solutions were prepared from a $\text{SrCl}_2 \cdot 6\text{H}_2\text{O}$ salt (99.995% trace metals basis, Sigma Aldrich). Stable Cs solutions were from CsCl (99.999% trace metals basis, Sigma Aldrich). ^{85}Sr and ^{137}Cs solutions were obtained from Cerca LEA (<https://www.orano.group/lea/fr>, France). Ionic strength was fixed using $\text{CaCl}_2 \cdot 4\text{H}_2\text{O}$ salt (99.995% Suprapure, Merck). The potassium nitrate amendment was simulated using KNO_3 ($\geq 99.0\%$, Sigma Aldrich).

2.2.2 Batch experiments

All experiments were carried out by batch method at room temperature ($22 \pm 2^\circ\text{C}$). They were performed in 10 mL polycarbonate Nalgene centrifuge tube (3138-0010, Thermo Scientific). All solutions and suspensions were prepared by weighing ($\sigma_m = 0.0005 \text{ mg}$).

Adsorption experiments were made with the $<150 \mu\text{m}$ fractions of soil samples. A mass of 0.35 g of soils was placed in centrifuge tubes with 7 mL of electrolyte to obtain a $50 \text{ g L}^{-1} \text{ S/L}$ ratio. As soils were mostly composed of exchangeable Ca^{2+} , the electrolyte solutions were prepared using a $0.033 \text{ mol kg}_w^{-1} \text{ CaCl}_2$, which is fixing the ionic strength to $I = 0.1 \text{ mol kg}_w^{-1}$. Soils were equilibrated under agitation with the CaCl_2 solution for 24 h ([Siroux et al., 2017a](#); [Siroux et al., 2018](#)). The pH values were controlled but not adjusted at this step. Stable SrCl_2 , or CsCl , were added in batches to reach an initial concentration range from 10^{-6} to 10^{-2} for Sr and 10^{-8} to $10^{-2} \text{ mol kg}_w^{-1}$ for Cs. Then, mixtures were spiked with ^{85}Sr or ^{137}Cs and left under agitation for two or five days for Sr and Cs, respectively.

The influence of an addition of KNO_3 to the solution — simulating an amendment to an agricultural soil — was done using slightly different conditions. From preliminary simulations using the MSIE parameters in [Siroux et al. \(2017a\)](#) and [Wissocq et al. \(2018\)](#), a higher S/L ratio of 0.25 kg L^{-1} and lower CaCl_2 concentrations of 1.5 and 2.5 mmol kg_w^{-1} for Sr and Cs, respectively, were chosen — the CaCl_2 concentrations were not the same as the selectivity coefficients are lower for Sr^{2+} and in order to be able to obtain measurable R_D changes. The added KNO_3 concentrations were 1 or 2 mmol kg_w^{-1} .

Suspensions were centrifuged (20,000 g during 45 min, 70.1 Ti Rotor, Optima LE-80R, Beckman), the pH values were checked, and 1 mL of the supernatant was collected and counted in gamma spectrometry.

The initial activities in the spiked experiments were determined using a blank procedure — same protocol but without soil samples in batches. The partition coefficients R_D ($L\ kg^{-1}$) were calculated using:

$$R_D = \left(\frac{C_i}{C_{eq}} - 1 \right) \cdot \frac{V}{m} \quad (1)$$

where C_i and C_{eq} are respectively the initial and equilibrium activities of Cs or Sr, V is the total volume of solution (L), and m is the total dry mass of solid phase (kg).

The partition coefficient R_D was chosen instead of distribution coefficient (K_D) because the reversibility of adsorption was not assessed.

2.2.3 Analytical methodology

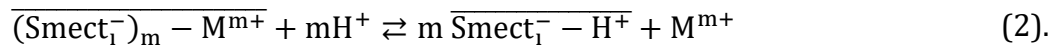
The measurement of the aqueous concentrations of stable Sr, Na, Ca, K, Mg, Al, and Si were carried out by ICP-AES (Activa, Horiba Jobin Yvon). Aliquots were diluted with 2% sub-boiling HNO_3 (DuoPur, Milestone) and measurements were made at 407.771 nm (Sr), 589.592 nm (Na), 317.933 nm (Ca), 766.490 nm (K), 273.553 nm (Mg), 167.020 and 396.152 nm (Al), and 212.412 nm (Si). The aqueous concentrations of Cs were measured by ICP-MS (Element 2, Thermo Fisher Scientific). The activities of supernatant were determined after sampling a 1 mL aliquot using a gamma counter (1480 Wizard 3, Perkin Elmer). The pH values were determined with a combined microelectrode (pH InLab, Mettler Toledo) through a redetermination of the Nernst plot of the electrode, and by calculating the pH value of the solutions from their measured potentials (buffer solutions 4.01, 7.00, and 9.18; Merck). Uncertainties from the linear regression are typically in the range of 0.05 pH-units.

2.3 Modelling and implementation of the database

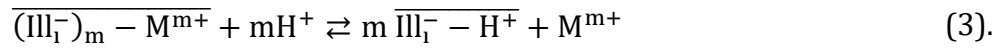
2.3.1 Multi-site ion-exchange model

The multi-site ion-exchange formalism has been developed elsewhere ([Motellier et al., 2003](#); [Reinoso-Maset and Ly, 2014](#); [Siroux et al., 2017a](#); [Siroux et al., 2018](#); [Wissocq et al., 2018](#)), and will only be recalled in the Supplementary Information.

The exchange equilibrium for the particular cases in this work are



for smectite sites Smect_i^- , and



for illite sites Ill_i^- , respectively.

The corrected selectivity coefficients $K_{M^{m+}/m\text{H}^+}^{*,X_i}$, are described as follows:

$$K_{M^{m+}/m\text{H}^+}^{*,X_i} = \frac{[\overline{X_i^- - \text{H}^+}]^m \cdot [M^{m+}]}{[\overline{(X_i^-)_m - M^{m+}}] \cdot [\text{H}^+]^m} \cdot \frac{\gamma_{M^{m+}}}{\gamma_{\text{H}^+}^m} \quad (4).$$

where X_i are the Smect_i and Ill_i sites, $[]$ is the solution concentration (mol kg^{-1} of water, mol kg_w^{-1}), $[\bar{}]$ is the adsorbed concentration (mol kg^{-1} of solid), and γ are the activity coefficient of aqueous species.

The site capacity is equal to the sum of all the adsorbed species concentrations. In a general notation, it is expressed as follows.

$$\text{SC}_i = [\overline{X_i^- - \text{H}^+}] + m[\overline{(X_i^-)_m - M^{m+}}] \quad (5)$$

2.3.2 Implementation of the database with K⁺ exchange parameters on illite and smectite

As a substantial amount of K will be added in one of the adsorption experiments (c.f. § 3.5), the K⁺/H⁺ selectivity coefficients have to be implemented to the database for Smect_i⁻ and Ill_i⁻ sites. The implementation strategy followed the principal steps presented in Siroux et al. ([2017a](#); [2018](#)): i) compilation of experimental results from the literature obtained on homo-ionic exchanger; ii) simultaneously fitting the model to these experimental data using the MS Excel Solver; and iii) determination of the uncertainties of the fitted parameters using the SolverAid macro ([De Levie, 2004](#)).

[Gaucher \(1998\)](#) has studied the saturation of a purified K-bentonite at $I = 0.02 \text{ mol L}^{-1}$ (KCl) and $S/L = 8 \text{ g L}^{-1}$ (Fig. 1a), and of a K-illite at $I = 0.02 \text{ mol L}^{-1}$ (KCl) and $S/L = 20 \text{ g L}^{-1}$ (Fig. 1b). [Missana et al. \(2014\)](#) have studied the adsorption at trace level of Cs onto K-illite. This latter study is particularly interesting because it permits determining the behaviour of K⁺ in the low concentration site Ill₀. For the sake of consistency, the site capacities from [Siroux et al. \(2017a\)](#) and [Wissocq et al. \(2018\)](#) in Table 1 have been used without further adjustment.

[Gaucher \(1998\)](#) proposed a CEC of 92.4 meq 100g⁻¹ for the purified bentonite. However, it appears that K⁺ did not saturate the CEC. The adsorbed K⁺ reached a maximum of 63 meq 100g⁻¹ in the pH range. Nevertheless, the simulation follows well the experimental data. The obtained selectivity coefficients are shown in Table 1.

The experimental data in Fig.1 are represented together with the modelling and the contribution of the different sites. The Ill₀ site is not represented in Fig. 1b as its concentration is very low (0.11 meq 100g⁻¹), and does not influence the K⁺ saturation of the exchanger vs. pH.

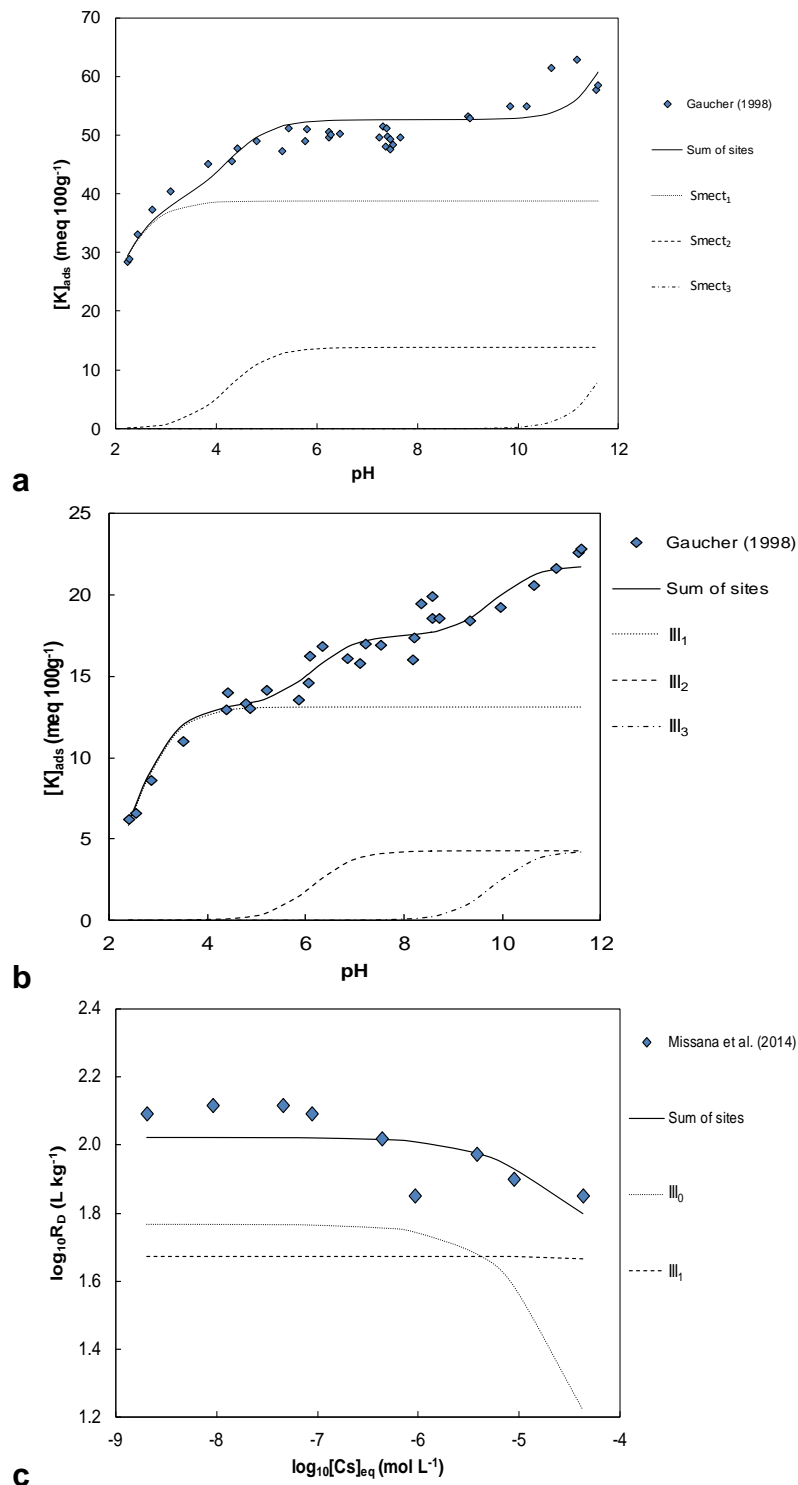


Fig. 1. Modelling of (a) the saturation of a bentonite with K^+ vs. pH at constant $I = 0.02$ mol L $^{-1}$ (KCl) and solid/liquid ratio (S/L) of 8 g L $^{-1}$ from [Gaucher \(1998\)](#); (b) the saturation of an illite with K^+ vs. pH at constant $I = 0.02$ mol L $^{-1}$ (KCl) and solid/liquid ratio (S/L) of 20 g L $^{-1}$ from [Gaucher \(1998\)](#); (c) the adsorption isotherm of Cs^+ onto K-illite at $I = 0.1$ mol L $^{-1}$ (KCl), pH 7 and S/L = 2 g L $^{-1}$ from [Missana et al. \(2014\)](#).

In the case of K-bentonite, even though the obtained selectivity coefficients are showing relatively low uncertainties, they could be questioned. The saturation curve does not reach the announced CEC (92.4 meq 100g⁻¹) and its underestimation is probably caused by an incomplete conditioning or difficulties in the experiment. Thus, the obtained corrected selectivity coefficient from this saturation curve must be considered with caution. Despite these problems, these values will be used in § 3.5 in order to test the predictive character of the both the modelling and the exchange parameter database.

The adsorption isotherm of Cs onto K-illite is presented in Fig. 1c showing the importance of Ill₀ site at trace concentration of Cs. In our database, the CEC of illite is at 24.9 meq 100 g⁻¹ while [Missana et al. \(2014\)](#) proposed a CEC of 19 meq 100g⁻¹.

All experiments were fitted simultaneously in order to obtain a coherent database. The selectivity coefficients obtained from these experiments are shown in Table 1. From the Cs⁺/H⁺ selectivity coefficients, and in order to compare with literature, the selectivity coefficient of K⁺/Cs⁺ exchange on the Ill₀ site, $\log_{10}K_{K^+/Cs^+}^{*,Ill_0}$, is calculated as follows,

$$\log_{10}\left(K_{K^+/Cs^+}^{*,Ill_0}\right) = \log_{10}\left(K_{K^+/H^+}^{*,Ill_0}\right) - \log_{10}\left(K_{Cs^+/H^+}^{*,Ill_0}\right) = 3.77 \pm 1.00 \quad (6)$$

which compares favourably with the one obtained by [Missana et al. \(2014\)](#), i.e. $\log\left(\frac{Cs}{K}K^{FES}\right) = 4.00 \pm 0.15$.

2.3.3 Database

The exchange parameters (SC_i and $\log_{10}\left(K_{M^+/N^+}^{*,X_i}\right)$) needed to carry out the simulations of Sr and Cs adsorption onto the soil samples were taken from [Wissocq et al. \(2018\)](#), where the adsorption behaviour of Cs⁺ and Sr²⁺ were studied onto Ca-conditioned smectite and illite in the MSIE formalism. As Ca²⁺ is the major exchangeable cation in all soil samples, it seems

preferable to use the Ca-database instead of the Na-database proposed in [Siroux et al. \(2018\)](#).

All parameters used for simulations are recalled in Table 1.

The exchange parameters of major cations and Cs^+ onto an Na-kaolinite according to the MSIE formalism were taken from [Reinoso-Maset and Ly \(2014\)](#). The authors reported the specific adsorption behaviour of Cs^+ at the lowest exchange capacity site X_s . The $\log_{10}\left(K_{\text{Cs}^+/\text{H}^+}^{*i,X_s}\right)$ was determined, but not the behaviour of Ca^{2+} on this site. We have assumed that Ca^{2+} would also saturate this binding site at whatever pH value and, consequently, the maximal value of $\log_{10}\left(K_{\text{Ca}^{2+}/2\text{H}^+}^{*,X_s}\right)$ was supposed to be nil — i.e., $K_{\text{Ca}^{2+}/2\text{H}^+}^{*,X_s} = 1$.

Experimental results on adsorption of Sr^{2+} onto kaolinite are particularly scarce in the literature. [Samadfam et al. \(2000\)](#) worked with an unconditioned kaolinite and did not specify its purity. [Ning et al. \(2017\)](#) studied the adsorption of Sr^{2+} onto an Na-kaolinite and obtained K_D between 600 and 40,000 L kg^{-1} (or mL g^{-1}), i.e. $\log_{10}K_D$ between 2.8 and 4.6 at ionic strength between 10 and 0.1 mmol L^{-1} NaCl and pH 4. The effect of pH was only studied at two pH values, and thus cannot be verified. [Rafferty et al. \(1981\)](#) studied the adsorption of Sr^{2+} onto an Na-kaolinite at different ionic strength fixed by sodium acetate at only at pH 5. Neglecting the possible difference in behaviour of Sr^{2+} onto Na- or Ca-kaolinite, the $\log_{10}R_D$ is low enough — at $I = 0.1 \text{ mol L}^{-1}$, $\log_{10}R_D$ ca. 1.6 at pH 7 compared to $\log_{10}R_D = 2.1$ for smectite at $I = 0.1 \text{ mol kg}_w^{-1}$ ([Siroux et al. 2017a](#)) and $\log_{10}R_D = 1.8$ for illite ([Poinsot et al. 1999b](#)) — that the adsorption of Sr^{2+} onto soils should not be significantly influenced by kaolinite and thus will not be further considered in the database for an operational modelling.

Table 1. Site capacities and selectivity coefficients used in this study.

Mineral	Site	Site capacity (meq 100g ⁻¹)	Selectivity coefficient	Selectivity coefficient value	References
Illite	Ill ₀	0.1	$\log_{10}K_{Ca^{2+}/2H^+}^{*,Ill_0}$	0.40 ± 1.98	Wissocq et al. (2018)
			$\log_{10}K_{Sr^{2+}/2H^+}^{*,Ill_0}$	-1.70 ± 1.82	Wissocq et al. (2018)
			$\log_{10}K_{Cs^+}/H^+^{*,Ill_0}$	-5.68 ± 1.00	Wissocq et al. (2018)
			$\log_{10}K_{K^+}/H^+^{*,Ill_0}$	-1.91 ± 0.12	Present work
	Ill ₁	13.1 ± 0.8	$\log_{10}K_{Ca^{2+}/2H^+}^{*,Ill_1}$	2.17 ± 0.07	Wissocq et al. (2018)
			$\log_{10}K_{Sr^{2+}/2H^+}^{*,Ill_1}$	2.43 ± 0.64	Wissocq et al. (2018)
			$\log_{10}K_{Cs^+}/H^+^{*,Ill_1}$	-0.85 ± 0.51	Wissocq et al. (2018)
			$\log_{10}K_{K^+}/H^+^{*,Ill_1}$	0.70 ± 0.12	Present work
	Ill ₂	4.3 ± 0.8	$\log_{10}K_{Ca^{2+}/2H^+}^{*,Ill_2}$	4.31 ± 0.22	Wissocq et al. (2018)
			$\log_{10}K_{Sr^{2+}/2H^+}^{*,Ill_2}$	3.68 ± 0.37	Wissocq et al. (2018)
			$\log_{10}K_{Cs^+}/H^+^{*,Ill_2}$	> 4.9 ^a	Wissocq et al. (2018)
			$\log_{10}K_{K^+}/H^+^{*,Ill_2}$	4.32 ± 0.18	Present work
	Ill ₃	7.4 ± 1.5	$\log_{10}K_{Ca^{2+}/2H^+}^{*,Ill_3}$	11.74 ± 0.20	Wissocq et al. (2018)
			$\log_{10}K_{Sr^{2+}/2H^+}^{*,Ill_3}$	11.25 ± 0.71	Wissocq et al. (2018)
			$\log_{10}K_{Cs^+}/H^+^{*,Ill_3}$	> 13.8 ^a	Wissocq et al. (2018)
$\log_{10}K_{K^+}/H^+^{*,Ill_3}$			7.98 ± 0.27	Present work	
Smectite	Smect ₀	0.01	$\log_{10}K_{Ca^{2+}/2H^+}^{*,Smect_0}$	-1.46 ± 0.58	Wissocq et al. (2018)
			$\log_{10}K_{Sr^{2+}/2H^+}^{*,Smect_0}$	-	Wissocq et al. (2018)
			$\log_{10}K_{Cs^+}/H^+^{*,Smect_0}$	-3.85 ± 0.27	Wissocq et al. (2018)
			$\log_{10}K_{K^+}/H^+^{*,Smect_0}$	-	Wissocq et al. (2018)
	Smect ₁	38.7 ± 3.8 ^b	$\log_{10}K_{Ca^{2+}/2H^+}^{*,Smect_1}$	0.49 ± 0.49	Wissocq et al. (2018)
			$\log_{10}K_{Sr^{2+}/2H^+}^{*,Smect_1}$	0.31 ± 0.03	Wissocq et al. (2018)
			$\log_{10}K_{Cs^+}/H^+^{*,Smect_1}$	-0.65 ± 0.08	Wissocq et al. (2018)
			$\log_{10}K_{K^+}/H^+^{*,Smect_1}$	-0.06 ± 0.12	Present work
	Smect ₂	36.1 ± 6.8 ^b	$\log_{10}K_{Ca^{2+}/2H^+}^{*,Smect_2}$	4.35 ± 0.03	Wissocq et al. (2018)
			$\log_{10}K_{Sr^{2+}/2H^+}^{*,Smect_2}$	4.47 ± 0.09	Wissocq et al. (2018)
			$\log_{10}K_{Cs^+}/H^+^{*,Smect_2}$	> 7.8 ^a	Wissocq et al. (2018)
			$\log_{10}K_{K^+}/H^+^{*,Smect_2}$	10.26 ± 0.14	Present work
	Smect ₃	13.9 ± 9.8 ^b	$\log_{10}K_{Ca^{2+}/2H^+}^{*,Smect_3}$	14.84 ± 0.06	Wissocq et al. (2018)
			$\log_{10}K_{Sr^{2+}/2H^+}^{*,Smect_3}$	14.78 ± 0.22	Wissocq et al. (2018)
			$\log_{10}K_{Cs^+}/H^+^{*,Smect_3}$	> 13.5 ^a	Wissocq et al. (2018)
$\log_{10}K_{K^+}/H^+^{*,Smect_3}$			2.39 ± 0.22	Present work	
Kaolinite	X _s	8.2.10 ⁻³	$\log_{10}K_{Ca^{2+}/2H^+}^{*,X_s}$	< 0 ^c	Reinoso-Maset and Ly (2014)
			$\log_{10}K_{Cs^+}/H^+^{*,X_s}$	-2.904 ± 0.001	Reinoso-Maset and Ly (2014)
	Y ₁ OH	1.08 ± 0.01	$\log_{10}K_{Ca^{2+}/2H^+}^{*,Y_1OH}$	0.329 ± 0.083	Reinoso-Maset and Ly (2014)
			$\log_{10}K_{Cs^+}/H^+^{*,Y_1OH}$	-0.10 ± 0.02	Reinoso-Maset and Ly (2014)
	Y ₂ OH	1.90 ± 0.01	$\log_{10}K_{Ca^{2+}/2H^+}^{*,Y_2OH}$	2.71 ± 0.01	Reinoso-Maset and Ly (2014)
			$\log_{10}K_{Cs^+}/H^+^{*,Y_2OH}$	3.62 ± 0.01	Reinoso-Maset and Ly (2014)

a. Upper limit values as very high uncertainties were attributed to several selectivity coefficients of caesium. These uncertainties were explained by the absence of fitting constraints ([Wissocq et al., 2018](#)) — these adsorption sites were not useful to model the experimental isotherms. Nonetheless, as the adsorption of Cs⁺ onto soils is generally driven by high affinity sites of illite, these adsorption sites should have a minimal influence on the adsorption behaviours.

b. Value from [Siroux et al. \(2017a\)](#).

c. Guessed value. See text for details.

Concerning chlorite, no adsorption studies are reported in the literature. Given its low cation-exchange capacity — 10-40 meq 100g⁻¹ ([Yong et al., 2012](#)) —, and the lack of knowledge of any specific behaviour for Cs⁺ or Sr²⁺, chlorite was neglected in the following.

3 RESULTS & DISCUSSION

3.1 Characterization of soil samples

Granulometric analyses, organic matter (OM) content, organic carbon and nitrogen concentrations, pH_{water} and pH_{KCl} , and $CaCO_3$ concentration of soils are reported in Table 2. All the samples showed a comparable percentage of fine particles (0-2 μm) referenced as clays.

Table 2. Granulometric analyses, natural organic matter (NOM), organic carbon (C_{org}), nitrogen, pH_{water} and pH_{KCl} , and $CaCO_3$ composition of soil samples (<2 mm).

	Depth	Clay (%)	Fine silt (%)	Coarse silt (%)	Fine sand (%)	Coarse sand (%)	OM	pH_{water}	pH_{KCl}	$CaCO_3$
	cm	0-2 μm	2-20 μm	20-50 μm	50-200 μm	200-2000 μm	$g\ 100g^{-1}$			$g\ 100g^{-1}$
Cambisol fluvic	0-30	16.5	19.5	16.7	18.4	28.9	4.39	6.9	7.1	3.5
Calcosol	0-20	18.2	13.8	33.5	27.3	7.2	2.03	7.5	7.4	4.9
Cambisol typic	0-14	13.1	18.9	35.2	21.0	11.8	4.94	5.5	4.7	1.4

The CEC of the less than 150 μm and 2 mm fractions showed similar values (Table 3). It suggests that the soil reactive components remained in the same proportions in both soil fractions and their repartitions in each soils were unaffected by the dry sieving. The less than 150 μm fractions can be considered as representative of the bulk soils (<2mm). For the sake of sample homogeneity, the <150 μm fractions were used for the experiments. However, the CEC measured with <150 μm material is not directly equal to the classical expression,

$$CEC_{soil} = CEC_{<2\mu m} p_{<2\mu m} + CEC_{NOM} p_{NOM} \quad (7)$$

where CEC_{soil} , $CEC_{<2\mu m}$, and CEC_{NOM} are the cation exchange capacities of the soil, less than 2 μm fraction, and NOM, respectively; $p_{<2\mu m}$ and p_{NOM} are the proportions of less than 2 μm fraction and NOM, respectively.

The CEC_{soil} value strongly depends on the selected CEC value for NOM, here estimated at $100 \text{ meq } 100g_{MO}^{-1}$. This classical relationship is only verified for the cambisol typic, i.e. $7.64 \text{ meq } 100g^{-1}$, compared to $7.56 \text{ meq } 100g^{-1}$. In case of cambisol fluvic, CEC_{soil} may yield reactive phases included in coarsest granulometric fractions — $12.2 \text{ meq } 100g^{-1}$ compared to $8.18 \text{ meq } 100g^{-1}$ — whereas NOM seems to be inhibited by cation saturation and pH conditions for calcosol — $9.89 \text{ meq } 100g^{-1}$ compared to $11.1 \text{ meq } 100g^{-1}$. Consequently, reactive phases proportions cannot be determined directly with the product of clay fraction percentage with $CEC_{<2\mu m}$. Hence, clay mineral proportion have to be estimated based on the CEC_{soil} after soil organic matter removal.

The exchangeable cations (Na^+ , K^+ , Ca^{2+} , Mg^{2+}) of these untreated fractions were then measured and compared to the soil dry-sieved at 2 mm (Table 3). The sum of exchangeable cations is representing 75, 102, and 66% of the CEC for the cambisol fluvic, cambisol, and cambisol typic, respectively. The greater difference for the cambisol typic reflects the exchangeable H^+ , which is present as expected for an acidic soil. Moreover, the soil OM contribution in the CEC is usually assumed to compensate the loss of exchangeable cation compared to the CEC. Indeed, after removal of NOM from $<150 \mu m$ material, the CEC were measured respectively at 10.4, 9.6, and $7.1 \text{ meq } 100g^{-1}$ for the cambisol fluvic, calcosol, and cambisol typic, respectively (Table 3 and 8). The removal of NOM does not largely change the CEC of soil samples except for the cambisol fluvic.

Table 3. Exchangeable cations concentrations and CEC measurement of soil samples (<150 µm) compared to the CEC of bulk soils (<2 mm).

Sample	Exchangeable cations (meq 100g ⁻¹)						Sum of exchangeable cations	CEC <150µm (meq 100g ⁻¹)	CEC <2mm (meq 100g ⁻¹)
	Cations	Na	Ca	Mg	K	Al			
Cambisol fluvic		0.08	8.09	0.40	0.70	-	9.27	12.41	12.2
Calcosol		0.08	9.25	0.22	0.40	-	9.95	9.78	9.89
Cambisol typic		0.24	2.44	0.52	0.36	1.43 ^a	4.99	7.53	7.64

^a Al concentration obtained on <2 mm fraction, extracted by KCl 1 M

The removal of Al led to an increase of the CEC of cambisol typic. It seemed that the CEC measurement protocol used in this study was not sufficient to remove completely the exchangeable Al from untreated samples. Therefore, the measured CEC on bulk cambisol typic soil sample and after removal of NOM were probably underestimated.

Contribution of reactive soil minerals was estimated based on their quantification in soil clay fraction. Reactive phases were limited to clay minerals, illite, smectite, kaolinite and chlorite. In the studied soil, only illite and smectite were present in mixed layer (I/S). Therefore, the proportion of illite and smectite took into account they repartition in the mixed layer. The CEC balance accounting all clay minerals have to be similar to this measured. Percentage of every phase was then calculated for minimum, average and maximum proportion (XRD quantification) and the resulting CEC was compared to the measured CEC. The closest CEC values were retained to select the proportion of phase mixture — the difference to 100% represented the non-reactive phases (quartz, feldspar...) not required for the model. The mineralogical composition (averaged mineral proportion) and the CEC of the <2 µm soil fractions are shown in Table 4.

Table 4. Average of the mineralogical proportion (in %) of the <2 μm fraction of the cambisol fluvic, calcosol, and cambisol typic.

Sample	mica, illite, glauconite	I/S R=1, G/S R=1	I/S R=0, G/S R=0	kaol.	chlorite ± C/S	quartz	feldsp. K	plagio-clases	goeth/Fe-mx	gyps.	TiO ₂
Cambisol fulvic	8.6 <i>8-11</i>	25.6 <i>21-31</i>	-	22.8 <i>18-23</i>	4.5 <i>0-7</i>	30 <i>26-31</i>	0.2 <i>0-1</i>	0.5 <i>0-1</i>	7.1 <i>3-8</i>	-	0.7 <i>0-0.7</i>
Calcosol	17.9 <i>14-25</i>	45.7 <i>40-50</i>	-	10.3 <i>9-12</i>	1.8 <i>0-4</i>	3.1 <i>2-6</i>	0.3 <i>0-2</i>	0.4 <i>0-1</i>	20.2 <i>15-22</i>	<0.1 <i>0-1</i>	0.3 <i>0-0.4</i>
Cambisol typic	14.5 <i>11-22</i>	50.5 <i>43-56</i>	-	20 <i>14-23</i>	2.1 <i>0-7</i>	5.3 <i>3-9</i>	0.2 <i>0-1</i>	0.4 <i>0-1</i>	6.2 <i>3-7</i>	<0.1 <i>0-1</i>	0.8 <i>0-0.9</i>

Abbreviations: mica, illite, glauconite: mica, illite and mixed layer (<20 % of smectite); I/S R=1: ordered mixed layer illite/smectite; I/S R=0: disordered mixed layer illite/smectite; G/S R=1: ordered mixed layer glauconite/smectite; I/S R=0: disordered mixed layer glauconite /smectite; kaol.: kaolinite; C/S: mixed layer chlorite/smectite; feldsp.K: potassium feldspar; goeth./Fe-mx: iron minerals (goethite, hematite, siderite, etc.); gyms. gypsum; TiO₂: titanium oxide.
Range of value is given in italic under the average value.

The cambisol fulvic contained an important proportion of quartz (30 %), which was subsequently be considered as a non-adsorbing phase for Cs⁺ and Sr²⁺. The illite/smectite ratio (I/S) was estimated following the position of the peak compared to the positions of peaks from discrete illite and smectite on the XRD diffractogram at the position (001). The mixed I/S layer ratio was estimated at I/S (40/60) for this soil. To simplify simulations and because it was not possible to distinguish mica and glauconite from illite, all these phases were considered as illite in a first approximation. The clay mineralogy was also described in terms of clay mineral types — illite, smectite, kaolinite and chlorite. Its clay mineral proportions are shown in Table 5. Considering also goethite with a CEC of 100 meq 100g⁻¹ (Langmuir, 1997) and by applying general CEC of 24.9 meq 100g⁻¹ for illite (Wissocq et al., 2018), 88.7 meq 100g⁻¹ for smectite (Siroux et al., 2017a), 5.6 meq 100g⁻¹ for kaolinite (Reinoso-Maset and Ly, 2014), 10 meq 100g⁻¹ for chlorite, the clay mineral quantification from the cambisol fluvic gave a CEC of 26.3 meq 100g⁻¹, close to the measured value of 22.9 meq 100g⁻¹.

Mixed layer I/S represents the major part of the reactive minerals in the <2 μm fraction of the calcosol. Moreover, more than 20% of goethite was quantified. Though goethite may slightly contribute to the CEC value in the <2 μm and untreated soil at pH value ca. 7.5, it was neglected in simulations of batch experiments in a first approximation. In light of the XRD diffractograms, three mixed layers were distinguished in a mixture of 6% I/S (10/90), 30% I/S (50/50) and

9.7% C/S (50/50). The calculated clay fraction proportions are shown in Table 5. These proportions allowed calculating a CEC of 52.2 meq 100g⁻¹.

The XRD pattern of the cambisol typic showed the presence of discrete mica or illite, which was considered as illite. Therefore, micaceous minerals were considered as illite. The 50.5% of mixed layers were interpreted as a mixture of 18.5% I/S (40/60) and 32% M/C (50/50). At pH_{water} = 5.5, goethite surface is supposed to be mainly positively charged — the point of zero charge varies from 7.5 to 9.3 ([Lyklema, 1995](#)) depending on carbonate content ([Villalobos and Leckie, 2000](#)) — and does not interfere in the CEC measurement. In consequence, these proportions represented a CEC of 22.6 meq 100g⁻¹, close to the measured CEC, i.e. 20 meq 100g⁻¹.

The clay mineral composition of each clay fraction was converted in proportion of pure mineral illite, smectite, kaolinite, and chlorite, and their associated CEC are shown in Table 5. As shown previously, the calculated CEC were similar to those measured for each soil samples.

As illite and smectite were both the most reactive phases for the adsorption of Cs⁺ and Sr²⁺, and importantly present, the compositions of soil samples were next simplified to illite/smectite (Table 5) and/or illite/smectite/kaolinite (Table 6) mixtures. In order to account for the contribution of other clay minerals in the CEC, illite and smectite proportions were re-evaluated by keeping the illite/smectite ratio constant (Table 6). The CEC of kaolinite being low compared to illite and smectite, the proportions of smectite and illite were unchanged overall considering or not the kaolinite contribution in the simulations.

Table 5. Calculated illite, smectite, kaolinite and chlorite proportions for each samples (<2 μm) and their associated calculated CEC.

Sample	Illite (%)	Smectite (%)	Kaolinite (%)	Chlorite (%)	Calculated CEC (meq 100g ⁻¹)	Measured CEC on <2 μm fraction (meq 100g ⁻¹)
Cambisol fluvic	18.8	14.4	22.8	4.5	26.3	22.9
Calcosol	33.5	25.25	10.5	6.65	52.2	49.7
Cambisol typic	37.9	11.1	20	18.1	22.6	20.0

Table 6. Total cation exchange capacities of the clay minerals ([Reinoso-Maset and Ly, 2014](#); [Wissocq et al., 2018](#)), and XRD-calculated proportions of illite, smectite, and kaolinite for soil samples (<150 μm after removal of NOM).

	Illite	Smectite	Kaolinite	Balanced CEC without Kaolinite	Balanced CEC with Kaolinite	Measured CEC
CEC (meq 100g ⁻¹)	24.9	88.7	3.0		(meq 100g ⁻¹)	
	XRD-calculated proportions in soils					
Cambisol fluvic	0.106	0.084	0.104	10.1	10.4	10.4
Calcosol	0.115	0.076	0.031	9.6	9.6	9.6
Cambisol typic	0.142	0.042	0.072	7.3	7.2	7.1

3.2 Simulation of Sr²⁺ and Cs⁺ adsorption onto soils

Adsorption isotherms in concentrations of Cs⁺ and Sr²⁺ were obtained onto untreated soil samples (<150 μm) at pH_{water} values and $I = 0.1 \text{ mol kg}_w^{-1} \text{ CaCl}_2$. To simplify the operational simulations, only clay minerals were considered as possible adsorbent of Cs⁺ and Sr²⁺, and the clay minerals proportion was first approximated to an illite/smectite mixture. Accounting for kaolinite in the operational simulation was also considered. Another simplification came from the fact that Ca²⁺ is the most concentrated major exchangeable cation in all soils, except for the cambisol typic. Soils were then considered initially saturated with calcium, and Ca²⁺ was the only major cation considered for simulations.

3.2.1 Adsorption of Cs⁺

The adsorption isotherms of Cs⁺ onto the soil samples at $I = 0.1 \text{ mol kg}_w^{-1}$ (CaCl₂) are shown on Fig. 2. Simulations of adsorption isotherms (plain line) and contributions from smectite and illite are also represented — the corresponding percentage of adsorption are shown in Fig. S2 of the SI. For every soil, isotherms were showing typical shape of Cs concentration isotherms onto illite ([Missana et al., 2014](#); [Poinssot et al., 1999a, b](#)) with the specific and strong adsorption at low concentrations generally attributed to the FES. From the clay mineral repartition for the adsorption of Cs⁺ on Fig. S2 of the SI, the adsorption was mainly dominated by illite. It is possible to claim that illite drove adsorption of Cs⁺ onto soils, especially for the cambisol fluvic and the calcosol.

The operational simulations followed satisfactorily the experimental results for the cambisol fluvic and calcosol. In terms of percentage of adsorption (see Fig. S2 of the SI), there was only a maximum overestimation of 9% for the cambisol fluvic and 11% for the calcosol. The presence of goethite in the calcosol was neglected, as it did not present any strong affinity for Cs⁺ under these pH conditions ([Ararem et al., 2011](#); [Jacquier et al., 2001](#); [Peynet, 2003](#)). In the case of the cambisol typic, the log₁₀R_D values of Cs were largely overestimated. This comment could be mitigated in term of percentage of adsorption onto which the overestimation is lower than 2% at low concentration.

The uncertainty of the simulations, calculated using the propagation of errors from selectivity coefficients and sites concentrations in Table 1, are shown on Fig. S4 of the SI — the uncertainty being the square root of the sum of the square of the residual between the simulation results using parameters in Table 1, and those obtained using the uncertainty for each implied selectivity coefficient and site capacity. The experimental adsorption isotherms were simulated satisfactorily for the cambisol fluvic and the calcosol, but the agreement was less satisfactory

for the cambisol typic, even accounting for the parameters uncertainty. The uncertainties on $\log_{10}\left(K_{\text{Ca}^{2+}/2\text{H}^+}^{*,\text{Ill}_0}\right)$ and $\log_{10}\left(K_{\text{Ca}^{2+}/2\text{H}^+}^{*,\text{Smect}_0}\right)$ (cf. Table 1) were driving the global uncertainty, particularly at low Cs concentration when the Ill₀ and Smect₀ were driving the adsorption phenomenon.

When kaolinite was taken into account (Fig. 2, dashed lines), the simulations were slightly lower at low concentration and higher at high concentrations. Kaolinite is a strong adsorbent for Cs⁺, but not strong enough to prevent illite and smectite from driving the adsorption process. Hence, considering kaolinite in the adsorption of Cs⁺ did not change the operational simulations significantly.

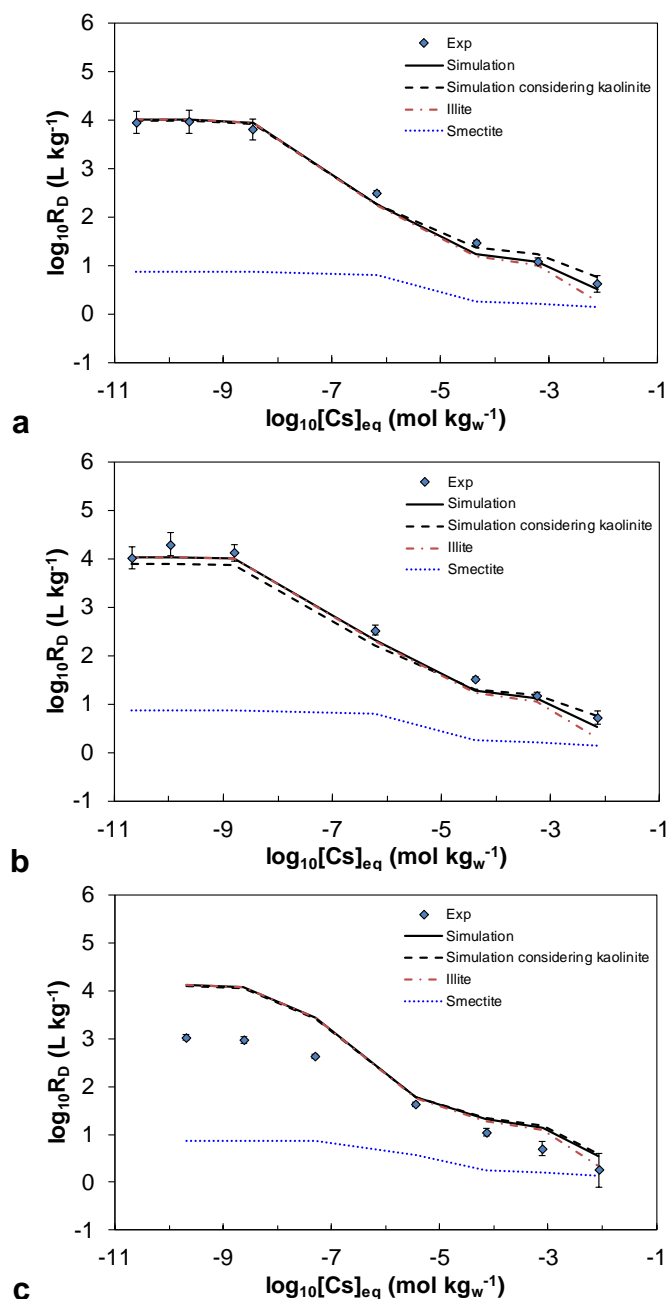


Fig. 2. Adsorption isotherms (partition coefficients vs. equilibrium concentration) of Cs⁺ onto soil samples at pH_{water} 6.4, 6.5, and 4.6 for the cambisol fluvic (a), calcosol (b), and cambisol typic (c), respectively; S/L = 50 g L⁻¹ and I = 0.1 mol kg_w⁻¹ (0.033 mol kg_w⁻¹ CaCl₂) with the associated simulations (black plain lines) and the contribution of smectite (blue dotted lines) and illite (red dash-dotted lines); error bars represent R_D uncertainty from activity counting; simulation accounting for kaolinite are shown in dashed lines.

Nevertheless, the agreement between experiments and simulations for the cambisol fluvic and calcosol indicated that the selectivity coefficients used for operational simulation can be used with confidence. It also seemed to confirm that the discrepancy between simulated and experimental $\log_{10}R_D$ value for the cambisol typic was not related to the selectivity coefficient uncertainties. This issue can come from several assumptions made for the cambisol typic. Experiments were carried out on untreated materials, but cambisol typic presented the highest amount of NOM (Table 7), which is known to obstruct the adsorption of Cs^+ in soils ([Dumat and Staunton, 1999](#); [Staunton et al., 2002](#)). Moreover, soils were considered as Ca-saturated, which was not the case for the cambisol typic (see Table 3). Indeed, competition between K^+ and Cs^+ in solution is depleting Cs adsorption onto illite ([Missana et al., 2014](#)). This soil also presented a large amount of exchangeable Al, which could be particularly difficult to exchange by monovalent cations as Cs^+ .

3.2.2 Adsorption of Sr^{2+}

Fig. 3 presents adsorption isotherms in concentration of Sr onto soils at pH_{water} and $I = 0.1 \text{ mol kg}_w^{-1}$ ($CaCl_2$). The contributions from smectite and illite in the simulation were also represented — the adsorption percentage onto soil samples and repartition between the different clay minerals is presented in Fig. S3 of the SI. The uncertainties of the simulation are shown in Fig. S5 of the SI.

The cambisol fluvic is a neutral soil ($pH_{water} = 6.9$) with a moderate concentration of limestone and organic matter. In solution, the dissolution of limestone could interfere in the adsorption of Sr through carbonate complexation. Nevertheless, using the minimum and maximum Sr concentration, i.e. $1 \text{ } \mu\text{mol kg}_w^{-1}$ and 7 mmol kg_w^{-1} , at the values of pH_{water} , and with the proportion of $CaCO_3$ of soils in Table 2, only minor amounts of $SrHCO_3^+$ - $SrCO_3(aq)$ can be calculated for the three soils — see Fig. S1a of the SI, where the inorganic speciation was

calculated using PhreeqC (version 3.4.0.12927; [Parkhurst and Appelo, 1999, 2013](#)) and the PRODATA database file ([Reiller and Descostes, 2020](#)) extracted for [Davies \(1962\)](#) equation of activity correction. The speciation calculations suggested that only at the highest added concentration of Sr, the cambisol typic and cambisol fluvic could have been oversaturated in strontianite (Fig. S1b of the SI).

Illite and smectite showed comparable affinities for Sr. Nevertheless, as smectite presented a higher CEC than illite, smectite tended to drive the adsorption onto soils. Sr $\log_{10}R_D$ values were slightly underestimated by simulations in the cases of the cambisol fulvic and calcosol, while it was slightly overestimated for the cambisol typic: in terms of percentage of adsorption, the highest overestimation was of 3.4% for the cambisol fluvic and 4.4% for the calcosol, and the adsorption was lowered to 3.7% for cambisol typic (Fig. S3 of the SI).

Assuming that the contribution of Ill₀ site of illite was minor, we only considered the uncertainties relative to other sites and principally to the high uncertainty associated to $\log_{10}\left(K_{Ca^{2+}/2H^+}^{*,Smect_1}\right)$ for smectite (cf. Table 1). This latter site had a minor role in the adsorption of Cs⁺, but a major one for Sr²⁺. Considering 2 σ uncertainty limits, the under and over estimations of the Sr adsorption did not seem to be significant (cf. Fig. S5 of the SI). In a first approximation, the selectivity coefficients and cation exchange capacities of the clay minerals can be used in the simulation of the adsorption onto a soil.

Particularly for the calcosol, goethite could be a good candidate to explain the difference between experimental results and operational simulation. [Hofmann et al. \(2005\)](#) observed a pH-edge between 6 and 8 for Sr²⁺ adsorption on a synthetic goethite at [NaNO₃] = 0.01 and 0.1 mol L⁻¹. Nevertheless, the role of goethite was neglected in our study due to the lack of previous studies exploitable within the MSIE formalism. A reinterpretation of adsorption data, e.g., recent data from [Hofmann et al. \(2005\)](#) and [Nie et al. \(2017\)](#), should be done as in Siroux et al.

([2017a](#); [2018](#)), [Wissocq et al. \(2018\)](#), and in this work (c.f. § 2.3.2 on the K^+/H^+ exchange on illite and smectite), if all necessary information for an MSIE fitting was available.

Contrary to the other soils, adsorption of Sr^{2+} onto cambisol typic was slightly overestimated. This difference could be attributed to the reasons exposed in § 2.3. Despite NOM does not strongly prevent the adsorption of Sr^{2+} in clay minerals ([Anjolaïya, 2015](#); [Samadfam et al., 2000](#)), as for Cs^+ , the presence of dissolved Al can influence the adsorption properties of clays ([Charlet et al., 1993](#); [Jardine et al., 1985](#); [Lutzenkirchen et al., 2014](#)), and then the adsorption of Sr^{2+} in soils — as it was shown for another alkaline earth metal cation such as Ca^{2+} ([Yang et al., 2003](#)).

The account of kaolinite (Fig. 3, dashed lines) did not change the operational simulations significantly for any of the soils.

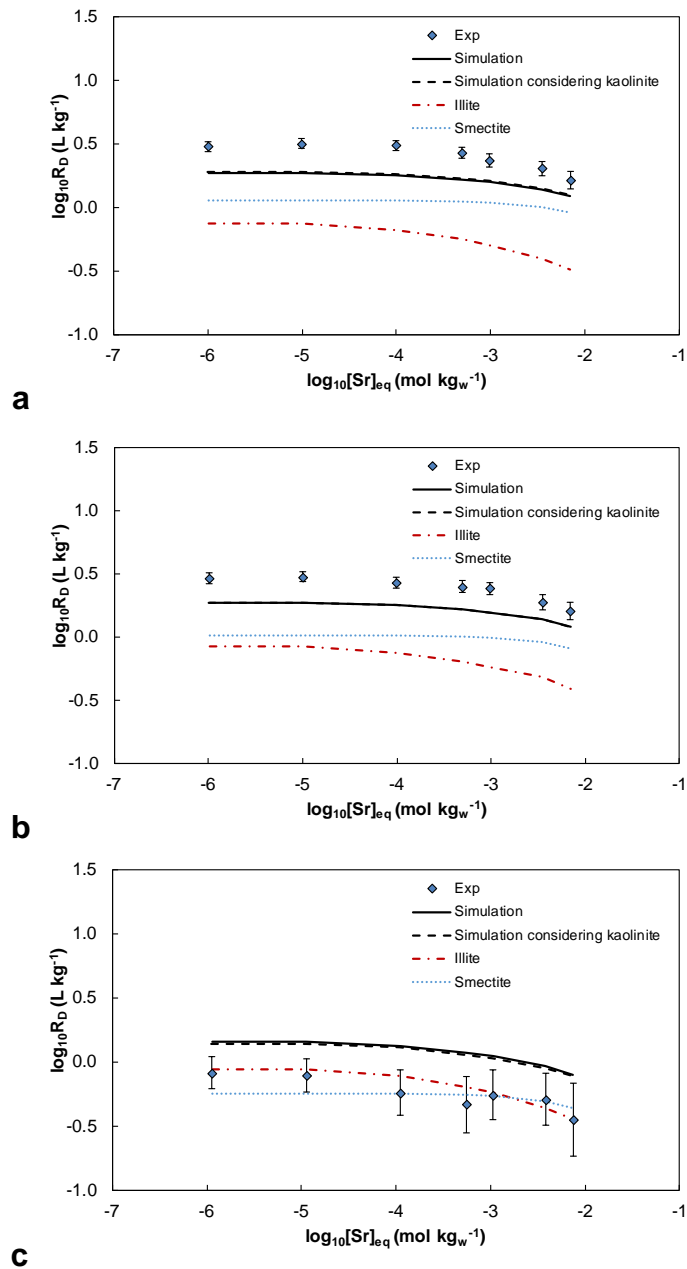


Fig. 3. Adsorption isotherms (partition coefficient vs. equilibrium concentration) of Sr²⁺ onto soil samples at pH_{water} 6.8, 7.1, and 4.8 for cambisol fluvic (a), calcosol (b), and cambisol typic (c), respectively; S/L = 50 g L⁻¹ and I = 0.1 mol kg_w⁻¹ (CaCl₂) with the associated simulations (plain lines) and the contributions from smectite (dashed line) and illite (dash-dotted lines); error bars represent R_D uncertainty from activity counting; simulations accounting for kaolinite are shown in dashed lines.

3.3 Removal of the natural organic matter

Natural organic matter is reported to affect the adsorption of caesium onto clay minerals by blocking the access of adsorption sites ([Staunton et al., 2002](#)). To study the effects of natural organic matter on the adsorption of Sr^{2+} and Cs^+ onto soils, NOM was removed from the soil samples (Table 7). After two steps, the removal was not total, but sufficient to appreciate an evolution in the adsorption behaviour of Sr^{2+} and Cs^+ . Moreover, the highest removal was observed on the most problematic cambisol typic.

Table 7. Concentration of natural organic matter in untreated soils and after removal of the fraction <150 μm .

Samples	Untreated material	After 2 H_2O_2 80°C treatments	% of C_{NOM} removal
	NOM ($\text{g}_{\text{NOM}} 100\text{g}^{-1}$)	NOM ($\text{g}_{\text{NOM}} 100\text{g}^{-1}$)	
Cambisol fluvic	4.30	0.80	81
Calcosol	2.91	0.95	67
Cambisol typic	4.21	0.31	93

The CEC and the exchangeable cation concentrations were checked in order to appreciate the basic properties of the treated materials (Table 8) compared to the untreated one (Table 6). The treatment has not modified the CEC of soil samples. The sum of exchangeable cations was comparable to the measured CEC except for the cambisol typic, the difference of which could be explained by the non-measurement of H^+ and exchangeable Al.

The adsorption isotherms of Cs^+ and Sr^{2+} onto soil samples after removing NOM were represented in Fig. 4 and 5. Adsorption isotherms of untreated materials were also represented for the sake of comparison. For Cs, as the Illo site of illite drove the simulations and as illite/smectite ratio stays constant, the CEC drop was therefore attributed only to the extracted NOM exchange capacity.

In Fig. 4 at low Cs concentration, the adsorption results after NOM removal onto the cambisol fluvic and calcosol were lower than the untreated material, but not significantly different. This concentration domain corresponded to the zone with the higher uncertainties for the experimental points that were due to the relatively high error on the activity counting — ranging from 10% at the lowest concentrations to 1% at the highest concentrations. Despite this slight reduction of $\log_{10}R_D$, the adsorption was assumed unchanged. For cambisol typic, the adsorption was the same with or without NOM removal.

Consequently, the influence of NOM did not permit to explain why the operational simulation did not follow the experimental points for this soil in the case of Cs. In our case, the removal of NOM has not changed significantly the adsorption behaviour of Cs⁺. Contrary to literature, adsorption of Cs⁺ did not seem to be affected by the removal of NOM for these soils. It is generally reported that the NOM impedes the adsorption of Cs⁺ onto clay mineral, especially illite, by blocking the access of frayed edge site ([Dumat and Staunton, 1999](#); [Staunton et al., 2002](#); [Tashiro et al., 2018](#)).

The Sr adsorption onto the calcosol and cambisol typic was mostly unchanged — at $[Sr]_{eq} = 1 \mu\text{mol kg}_w^{-1}$, the adsorption percentage increased at 3% for the calcosol and 1% for the cambisol typic. In the case of the cambisol fluvic, the adsorption of Sr²⁺ was slightly lowered, but not significantly in view of experimental uncertainties. For Sr, as illite and smectite showed similar adsorption behaviours, operational simulations were mostly driven by the CEC. Contrary to cambisol fluvic, the CEC values of the calcosol and cambisol typic have not significantly changed. Consequently, the removal of NOM did not seem to influence the adsorption of Sr²⁺ in these soils, which is in agreement with the literature ([Samadfam et al., 2000](#)).

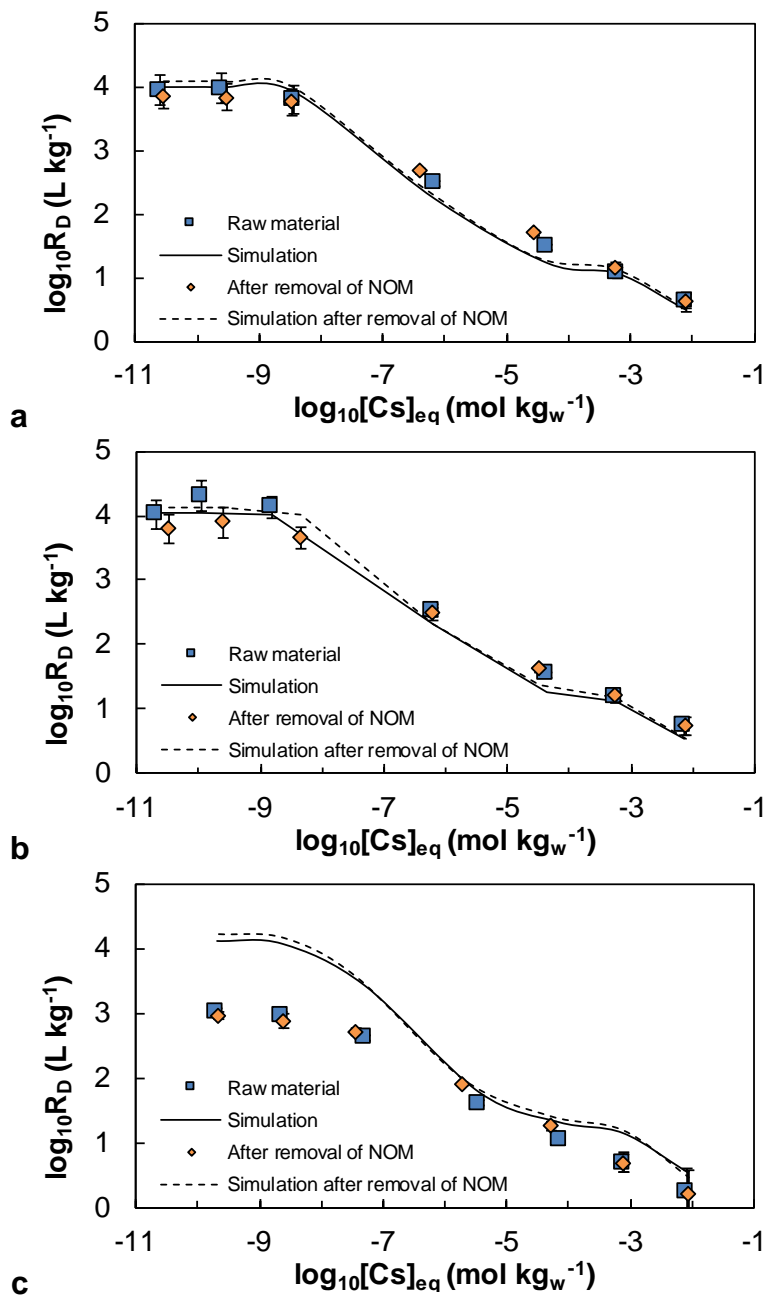


Fig. 4. Adsorption isotherms (partition coefficient vs. equilibrium concentration) of Cs^+ onto untreated soil samples (squares, simulation plain lines from Fig. 2) and after the removal of NOM (diamonds, simulation dashed lines) at pH_{water} 6.5, 6.8, and 5.2 for the cambisol fluvic (a), calcosol (b), and cambisol typic (c), respectively; $S/L = 50 \text{ g L}^{-1}$ and $I = 0.1 \text{ mol kg}_w^{-1}$ ($CaCl_2$); error bars represent R_D uncertainty from activity counting.

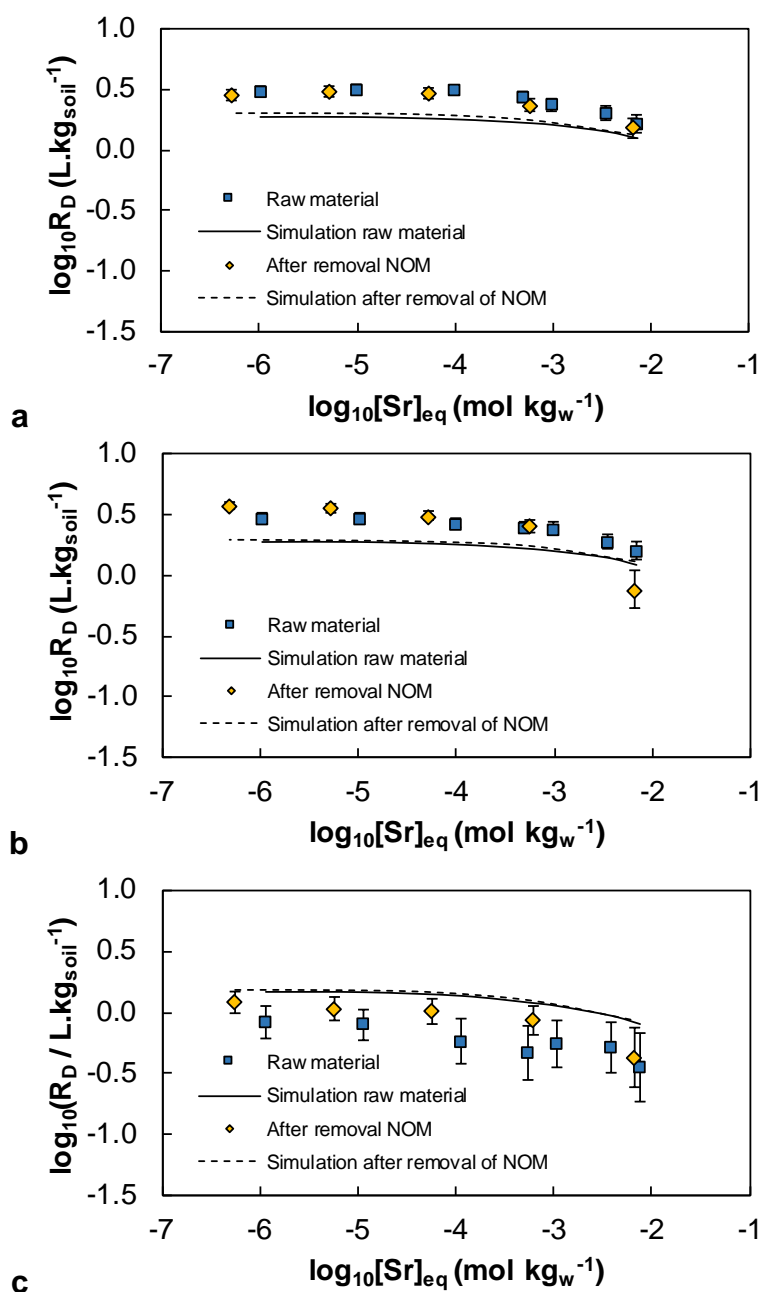


Fig. 5. Adsorption isotherms (partition coefficient vs. equilibrium concentration) of Sr²⁺ onto untreated soil samples (squares, simulation plain lines from Fig. 3) and after the removal of NOM (diamonds, simulation dashed lines) at pH_{water} 6.7, 7.2, and 5.2 for cambisol fluvic (a), calcosol (b), and cambisol typic (c), respectively; S/L = 50 g L⁻¹ and I = 0.1 mol kg_w⁻¹ (CaCl₂); error bars represent R_D uncertainty from the activity counting.

Table 8. Exchangeable cations concentrations and CEC measurement of <150 μm soil samples after removal of NOM and of cambisol typic after removal of aluminium.

Sample	Exchangeable cations (meq 100g ⁻¹)				Sum of exchangeable cations	CEC (meq 100g ⁻¹)
	Na	Ca	Mg	K		
<150 μm soil samples after removal of NOM						
Cambisol fluvic	0.05	10.26	0.35	0.35	11.01	10.40
Calcosol	0.08	8.90	0.16	0.74	9.86	9.58
Cambisol typic	0.05	2.24	0.34	0.21	2.85	7.08
Cambisol typic after removal of aluminium						
	0.05	9.20	0	0.32	9.61	10.1

3.4 Adsorption onto cambisol typic after removing the exchangeable aluminium

An important amount of exchangeable Al was found in this cambisol typic (Table 3): highly charged cations, $\text{Al}(\text{OH})_n^{(3-n)+}$ could be particularly difficult to be exchanged by Cs^+ and Sr^{2+} . The removal of the exchangeable Al on the cambisol typic soil enhanced the CEC (Table 8), but was not sufficient to extract all exchangeable Al.

The adsorption isotherms of Sr^{2+} and Cs^+ onto the cambisol typic after the Al removal and the corresponding simulations were represented in Fig. 6. For Sr^{2+} , the account for exchangeable aluminium in the simulations and experiments were in good agreement. For Cs^+ , the adsorption was slightly increased by the removal of Al but operational simulations still did not follow the experimental results, even though they were also increased. In Table 8, the consistency between the sum of the exchangeable cations and the measured CEC allowed assuming that exchangeable Al was removed effectively. This indicates that Al compensated exchangeable negative sites and limited Sr adsorption on these sites. However, it was possible that a very low concentration of Al remained in soil, specifically located on the Cs specific sites of illite. Therefore, the adsorption of Cs^+ onto these sites could remain impeded.

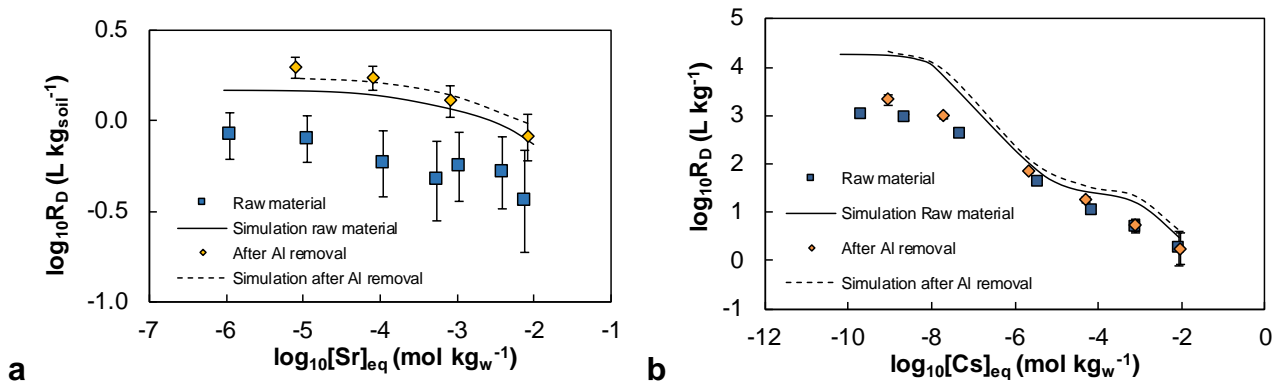


Fig. 6. Adsorption isotherms (partition coefficient vs. equilibrium concentration) of Sr (a) and Cs (b) onto cambisol typical (square, simulation plain line from Fig. 3 for Sr and Fig. 2 for Cs) and after the removal of exchangeable Al (diamonds, simulation dashed line) at $pH_{water} = 6$ (a) and 6.4 (b), $S/L = 50 \text{ g L}^{-1}$ and $I = 0.1 \text{ mol kg}_w^{-1}$ (CaCl₂).

3.5 Adsorption on the calcosol in a simplified synthetic pore water

The adsorption of Cs⁺ and Sr²⁺ onto the calcosol under closer to environmental conditions was simulated using the database. Under these conditions, K⁺ is another competitor for the access to fixation sites. Adsorption isotherms of Sr²⁺ and Cs⁺, and corresponding operational simulations were shown in Fig. 7. In both cases, the addition of KNO₃ in solution lowered the adsorption, as well as the resulting simulations.

Concerning adsorption of Sr²⁺ onto the calcosol in synthetic pore water (Fig. 7a), one must note that compared to the adsorption of Sr²⁺ onto the soils (§ 3.2.2), the ionic strength is lowered from 100 to 4.5 mmol kg_w⁻¹. The selectivity coefficients used for these simulations were determined at $I = 0.03 \text{ mol L}^{-1}$ by [Wissocq et al. \(2018\)](#). The simulation agreement could be altered when varying ionic strengths from this initial value, which can explain the underestimation at higher ionic strength ($I = 0.1 \text{ mol kg}_w^{-1}$), and the overestimation at lower ionic strength ($I = 4.5 \text{ mmol kg}_w^{-1}$). Moreover, the simulations were slightly overestimating the decrease of the adsorption of Sr²⁺ with KNO₃ addition in the synthetic pore water. One must

also note that ionic strength was slightly increasing with KNO_3 concentration (i.e., $I = 5.5$, and $6.5 \text{ mmol kg}_w^{-1}$, for $[\text{KNO}_3] = 1$ and 2 mmol kg_w^{-1} , respectively). Although operational simulations represented satisfactorily the experimental results, they could be further refined by improving the selectivity coefficients of K^+/H^+ exchange, which was out of the framework of this study.

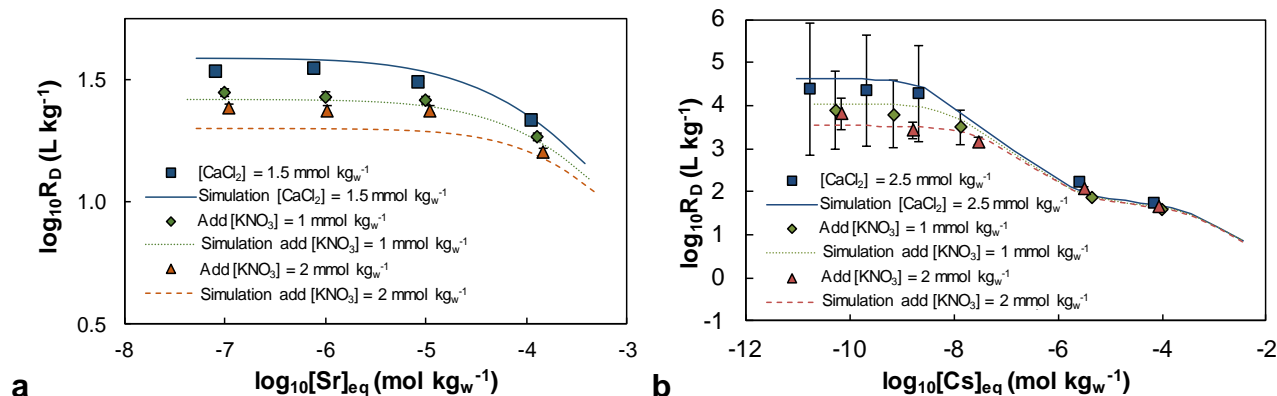


Fig. 7. Adsorption isotherm (partition coefficient vs. equilibrium concentration) onto the calcosol $S/L = 0.25 \text{ kg L}^{-1}$ of (a) Sr^{2+} at $\text{pH}_{\text{water}} = 7.2$, and $[\text{CaCl}_2] = 1.5 \text{ mmol kg}_w^{-1}$ ($I = 4.5 \text{ mmol kg}_w^{-1}$, squares, simulation plain line), addition of $[\text{KNO}_3] = 1 \text{ mmol kg}_w^{-1}$ ($I = 5.5 \text{ mmol kg}_w^{-1}$, diamonds, simulation dotted line), and addition of $[\text{KNO}_3] = 2 \text{ mmol kg}_w^{-1}$ ($I = 6.5 \text{ mmol kg}_w^{-1}$, triangles, simulation dashed line); and (b) of Cs^+ at $\text{pH}_{\text{water}} = 6.9$, and $[\text{CaCl}_2] = 2.5 \text{ mmol kg}_w^{-1}$ ($I = 7.5 \text{ mmol kg}_w^{-1}$, square, simulation plain line), addition of $[\text{KNO}_3] = 1 \text{ mmol kg}_w^{-1}$ ($I = 8.5 \text{ mmol kg}_w^{-1}$, diamonds, simulation dotted line), and addition of $[\text{KNO}_3] = 2 \text{ mmol kg}_w^{-1}$ ($I = 9.5 \text{ mmol kg}_w^{-1}$, triangles, simulation dashed line).

In the case of Cs^+ (Fig. 7b), the addition of KNO_3 in the synthetic pore water also imposed a decrease in adsorption. Due to the high affinity for FES, K^+ was in competition with Cs^+ onto these sites and the decrease was more important at low than at high Cs concentrations. The high uncertainties on the experimental points at low concentration showed that the experiment was probably not properly dimensioned. The S/L ratio and ionic strength were higher and lower with respect to Sr^{2+} experiment to increase the adsorption of Cs^+ (i.e., $I = 7.5, 8.5$, and 9.5

mmol kg_w⁻¹, for [KNO₃] = 0, 1, and 2 mmol kg_w⁻¹, respectively). However, the spiked activity of radioactive tracers was not changed. The activities at equilibrium were then too low to obtain an acceptable counting accuracy. Based on same reasons considered for Sr²⁺, one can assume that the increase in KNO₃ concentration, and thus in ionic strength, would reduce the difference between experimental and simulated R_D values, but to a much lower scale as the Ill₀ sites are particularly selective of Cs⁺. Nonetheless, operational simulations represented well both the adsorption of Cs⁺ at low ionic strength and the addition of K⁺.

Accounting for all the uncertainties generated by the calculated proportions on clay minerals and the selectivity coefficients used, the operational simulation using MSIE modelling seemed to predict satisfactorily the adsorption behaviour of Sr and Cs onto the calcosol under environmentally relevant conditions.

3.6 Comments on modelling and operational simulations accuracy

The operational simulation applying MSIE modelling with an additivity approach principle allowed representing satisfactorily the adsorption behaviour of Cs⁺ and Sr²⁺ onto these soil samples. Some parameters still limited the simulations. First, the uncertainty on the clay mineral proportions in soils were calculated from the average percentages. However, changes in these percentages can influence the simulation results: c.f. Fig. S2 and S3 of the SI.

Moreover, the difficulty to discriminate micaceous minerals from illite by XRD seemed to induce a problem in the simulations; particularly for the adsorption of Cs⁺. In our case, these minerals were combined because weathered micaceous minerals, as biotite or muscovite, are known to strongly adsorb Cs due to the presence of FES ([Zaunbrecher et al., 2015](#)). Nevertheless, this adsorption is not necessarily as strong as for illite. [Cornell \(1993\)](#) reviewed the adsorption in different clay minerals including illite, biotite, and muscovite, and reported lower adsorption of

Cs⁺ onto biotite than onto illite. The reported partition coefficient of Cs⁺ onto muscovite was also lower than the one for illite. Henceforth, to improve the operational simulation in the case of the cambisol typic, differentiate mica to illite would eventually be necessary.

Considering these soils as saturated with Ca is a strong assumption for the operational simulations. However, taking into account all the exchangeable cations (Na⁺, Mg²⁺, K⁺, etc.) would require a complete database of exchange parameters for each of these exchangeable cations in the framework of the MSIE model. Nonetheless, the good representation of the experimental results by operational simulation confirmed that the choice of considering these exchangers as Ca-saturated was correct, except for the cambisol typic.

In this study, the secondary minerals — i.e. quartz, feldspar, goethite, etc. — were neglected. This choice was made in view of their low CEC and their absence of specific adsorption behaviour for Cs⁺ and Sr²⁺. This was justified in the view of an operational modelling based on first order phenomena. [Cornell \(1993\)](#) reported weak adsorption of Cs⁺ onto quartz, chlorite, and albite (feldspar). Quartz is also reported as a weak adsorbent of Sr ([Nordén et al., 1994](#)). The case of goethite, and others iron oxo-hydroxides, which has already been discussed in § 3.1, does not represent a particularly strong adsorbent for Cs⁺, but seems to adsorb Sr²⁺ ([Fuller et al., 2016](#); [Hofmann et al., 2005](#); [Nie et al., 2017](#)). Having neglected goethite contribution may explain part of the differences between the experimental results and the operational simulations for the adsorption of Sr²⁺ onto soils, especially for the calcosol.

Finally, we saw that the removal of Al allowed us to simulate the adsorption behaviour of Sr²⁺ satisfactorily. Adding the selectivity coefficient of the Al system — i.e., $\text{Al}(\text{OH})_n^{(3-n)+} / (3-n)\text{H}^+$ — would allow improving the database and the prediction capacities of the operational modelling, but these studies are missing in the literature and difficult to obtain on phyllosilicate phases. In

our case, the lack of information on these exchanges was impeding a good representation of the adsorption behaviour on acidic soils, which contained dissolved Al.

The uncertainties of the used selectivity coefficients caused high uncertainties on simulations. Nevertheless, operational simulations represented satisfactorily the experimental results in most cases. It seems though that the proposed selectivity coefficients are suited in these cases.

4 CONCLUSIONS

The adsorption of caesium and strontium were studied onto French soil samples. These samples were approximated to illite/smectite or illite/smectite/kaolinite mixtures in order to propose an operational simulation of their adsorption behaviours and compare these operational simulations with experimental results. The database used for the simulations was taken from literature for illite and smectite ([Siroux et al., 2017a](#); [Wissocq et al., 2018](#)) or were adjusted in this study for kaolinite ([Reinoso-Maset and Ly, 2014](#)).

Operational simulations were carried out considering the additivity principle between several phases was the main influence on the adsorption of Sr and Cs. The simulations and experimental results were in agreement mainly for the cambisol fluvic and calcosol, thus confirming the efficiency of the database and the operational modelling to predict and represented the adsorption behaviour of Cs and Sr onto soils. In the case of the cambisol typic, the agreement between experimental $\log_{10}R_D$ values and operational simulations was not totally satisfactory, and the problem stays unresolved for the Cs^+ adsorption. Nevertheless, it can be moderated in view of the low differences in adsorption percentage. The presence of exchangeable Al in the case of Sr adsorption and uncertainties on the clay fraction determination (and the non-differentiation between mica and illite) for Cs adsorption were the main factors affecting the operational simulations of sorption onto soils.

These first results obtained on a relevant synthetic pore water on the calcosol are promising. Nevertheless, the database can be further improved by implementing the adsorption behaviour of other principal and secondary mineral phases (chlorite, goethite, quartz, etc.). Finally, this study confirms that the MSIE modelling allows to predict the adsorption of cations onto various soils from an operational point of view.

ACKNOWLEDGMENTS

This work was financed through the French “Programme Investissement d’Avenir” (ANR-11-RSNR-0005 DEMETERRES, <https://anr.fr/ProjetIA-11-RSNR-0005>). ORANO is acknowledged for its financial support. The authors thank the LAS (INRA Arras, France) and ERM (Poitiers, France) laboratories for their support on soils analyses; and IPGP multidisciplinary program PARI and Paris-IdF region SESAME Grant No. 12015908 for the organic matter determinations. An anonymous reviewer is acknowledged for his very detailed and constructive review.

REFERENCES

Adeleye, S.A., Clay, P.G., Oladipo, M.O.A., 1994. Sorption of cesium, strontium and europium ions on clay-minerals. *J. Mater. Sci.* 29, 954-958. DOI: 10.1007/bf00351416.

Anjolaia, O., 2015. Sorption behaviour of metal contaminants in clay minerals, soils and matrices: understanding the influence of organic matter, pH, ionic strength and mineralogy. PhD Thesis. Loughborough University, Loughborough, UK. pp. 280.

<http://dspace.lboro.ac.uk/dspace-jspui/bitstream/2134/17523/3/Thesis-2015-Anjolaia.pdf>.

Ararem, A., Bouras, O., Arbaoui, F., 2011. Adsorption of caesium from aqueous solution on binary mixture of iron pillared layered montmorillonite and goethite. *Chem. Eng. J.* 172, 230-236. DOI: 10.1016/j.cej.2011.05.095.

Baborova, L., Vopalka, D., Cervinka, R., 2018. Sorption of Sr and Cs onto Czech natural bentonite: experiments and modelling. *J. Radioanal. Nucl. Chem.* 318, 2257-2262. DOI: 10.1007/s10967-018-6196-3.

Bouchet, A., 1992. Mise au point d'un programme de détermination automatique des minéraux argileux, *Comptes Rendus du Colloque de Rayons X-Siemens*, pp. 52-61.

Bunzl, K., Kracke, W., Agapkina, G.I., Tikhomirov, A., Shcheglov, A.I., 1998. Association of Chernobyl derived $^{239+240}\text{Pu}$, ^{241}Am , ^{90}Sr and ^{137}Cs with different molecular size fractions of organic matter in the soil solution of two grassland soils. *Radiat. Environ. Biophys.* 37, 195-200. DOI: 10.1007/s004110050117.

Campbell, L.S., Davies, B.E., 1995. Soil sorption of caesium modelled by the Langmuir and Freundlich isotherm equations. *Appl. Geochem.* 10, 715-723. DOI: 10.1016/0883-2927(95)00056-9.

Charlet, L., Schindler, P.W., Spadini, L., Furrer, G., Zysset, M., 1993. Cation adsorption on oxides and clays: the aluminum case. *Aquat. Sci.* 55, 291-303. DOI: 10.1007/bf00877274.

Cornell, R., 1993. Adsorption of cesium on minerals: a review. *J. Radioanal. Nucl. Chem.* 171, 483-500. DOI: 10.1007/Bf02219872.

d'Orlyé, F., Reiller, P.E., 2012. Contribution of capillary electrophoresis to an integrated vision of humic substances size and charge characterizations. *J. Colloid Interface Sci.* 368, 231-240. DOI: 10.1016/j.jcis.2011.11.046.

Davies, C.W., 1962. Ion Association. Butterworths, Washington, DC, USA. pp. 190.

De Levie, R., 2004. Advanced Excel for Scientific Data Analysis. Oxford University Press, Oxford, UK.

Dumat, C., Cheshire, M.V., Fraser, A.R., Shand, C.A., Staunton, S., 1997. The effect of removal of soil organic matter and iron on the adsorption of radiocaesium. *Eur. J. Soil Sci.* 48, 675-683. DOI: 10.1111/j.1365-2389.1997.tb00567.x.

Dumat, C., Staunton, S., 1999. Reduced adsorption of caesium on clay minerals caused by various humic substances. *J. Environ. Radioact.* 46, 187-200.

Dumat, C., Quiquampoix, H., Staunton, S., 2000. Adsorption of cesium by synthetic clay-organic matter complexes: Effect of the nature of organic polymers. *Environ. Sci. Technol.* 34, 2985-2989.

Durrant, C.B., Begg, J.D., Kersting, A.B., Zavarin, M., 2018. Cesium sorption reversibility and kinetics on illite, montmorillonite, and kaolinite. *Sci. Total Environ.* 610-611, 511-520. DOI: <https://doi.org/10.1016/j.scitotenv.2017.08.122>.

Dyer, A., Chow, J.K.K., Umar, I.M., 2000. The uptake of caesium and strontium radioisotopes onto clays. *J. Mater. Chem.* 10, 2734-2740. DOI: 10.1039/B006662L.

Dzene, L., Tertre, E., Hubert, F., Ferrage, E., 2015. Nature of the sites involved in the process of cesium desorption from vermiculite. *J. Colloid Interface Sci.* 455, 254-260. DOI: 10.1016/j.jcis.2015.05.053.

Dzombak, D.A., Morel, M.M., 1990. Surface Complexation Modelling: Hydrous Ferric Oxide. John Wiley & Sons, New York, NY, USA. pp. 416.

England, T.R., Rider, B.F., 1993, ENDF-349 Evaluation and Compilation of Fission Product Yields, Lawrence Berkeley National Laboratory. Report LA-UR-3106. p. 173.

<http://t2.lanl.gov/nis/publications/endl349.pdf>.

Erten, H.N., Aksoyoglu, S., Hatipoglu, S., Gokturk, H., 1988. Sorption of cesium and strontium on montmorillonite and kaolinite. *Radiochim. Acta* 44/45, 147-151. DOI: 10.1524/ract.1988.4445.1.147.

Fujikawa, Y., Zheng, J., Cayer, I., Sugahara, M., Takigami, H., Kudo, A., 1999. Strong association of fallout plutonium with humic and fulvic acid as compared to uranium and ¹³⁷Cs in Nishiyama soils from Nagasaki, Japan. *J. Radioanal. Nucl. Chem.* 240, 69-74.

Fuller, A.J., Shaw, S., Peacock, C.L., Trivedi, D., Burke, I.T., 2016. EXAFS study of Sr sorption to illite, goethite, chlorite, and mixed sediment under hyperalkaline conditions. *Langmuir* 32, 2937-2946. DOI: 10.1021/acs.langmuir.5b04633.

Gaines, G.L., Thomas, H.C., 1953. Adsorption studies on clay minerals. II. A formulation of the thermodynamics of exchange adsorption. *J. Chem. Phys.* 21, 714-718. DOI: 10.1063/1.1698996.

Galamboš, M., Krajnak, A., Roskopfová, O., Viglasova, E., Adamcova, R., Rajec, P., 2013. Adsorption equilibrium and kinetic studies of strontium on Mg-bentonite, Fe-bentonite and illite/smectite. *J. Radioanal. Nucl. Chem.* 298, 1031-1040. DOI: 10.1007/s10967-013-2511-1.

Gaucher, E., 1998. Interactions eaux-argiles. Etude expérimentale. PhD Thesis. Université Denis Diderot (Paris VII), Paris, France. pp. 260. In French.

Goto, M., Rosson, R., Wampler, J.M., Elliott, W.C., Serkiz, S., Kahn, B., 2008. Freundlich and dual Langmuir isotherm models for predicting ¹³⁷Cs binding on Savannah River Site soils. *Health Phys.* 94, 18-32. DOI: 10.1097/01.HP.0000278416.04381.31.

Gutierrez, M., Fuentes, H.R., 1991. Competitive adsorption of cesium, cobalt and strontium in conditioned clayey soil suspensions. *J. Environ. Radioact.* 13, 271-282. DOI: 10.1016/0265-931X(91)90001-V.

Han, C.H., Park, Y.H., Lee, Y.G., Park, J.W., 2016. Distribution of ⁹⁰Sr activities in the environmental radiation samples of Jeju Island, Korea. *J. Radiat. Prot. Res.* 41, 418-423. DOI: 10.14407/jrpr.2016.41.4.418.

Hayes, G.P., Meyers, E.K., Dewey, J.W., Briggs, R.W., Earle, P.S., Benz, H.M., Smoczyk, G.M., Flamme, H.E., Barnhart, W.D., Gold, R.D., Furlong, K.P., 2017, Tectonic summaries of magnitude 7 and greater earthquakes from 2000 to 2015, U.S. Geological Survey, Reston, VA, USA. Report 2016-1192. p. 148. <http://pubs.er.usgs.gov/publication/ofr20161192>.

Hofmann, A., van Beinum, W., Meeussen, J.C.L., Kretzschmar, R., 2005. Sorption kinetics of strontium in porous hydrous ferric oxide aggregates II. Comparison of experimental results and model predictions. *J. Colloid Interface Sci.* 283, 29-40. DOI: 10.1016/j.jcis.2004.08.105.

Hou, X.L., Fogh, C.L., Kucera, J., Andersson, K.G., Dahlgaard, H., Nielsen, S.P., 2003. Iodine-129 and caesium-137 in Chernobyl contaminated soil and their chemical fractionation. *Sci. Total Environ.* 308, 97-109. DOI: 10.1016/S0048-9697(02)00546-6.

Jacquier, P., Meier, P., Ly, J., 2001. Adsorption of radioelements on mixtures of minerals — experimental study. *Appl. Geochem.* 16, 85-93. DOI: 10.1016/S0883-2927(00)00022-6.

Jacquier, P., Ly, J., Beaucaire, C., 2004. The ion-exchange properties of the Tournemire argillite: I. Study of the H, Na, K, Cs, Ca and Mg behaviour. *Appl. Clay Sci.* 26, 163-170. DOI: 10.1016/j.clay.2003.09.009.

Jardine, P.M., Zelazny, L.W., Parker, J.C., 1985. Mechanisms of aluminum adsorption on clay minerals and peat. *Soil Science Society of America Journal* 49, 862-867. DOI: 10.2136/sssaj1985.03615995004900040015x.

Kanda, J., 2013. Continuing ^{137}Cs release to the sea from the Fukushima Dai-ichi Nuclear Power Plant through 2012. *Biogeosciences* 10, 6107-6113. DOI: 10.5194/bg-10-6107-2013.

Karamalidis, A.K., Dzombak, D.A., 2010. *Surface Complexation Modeling: Gibbsite*. John Wiley & Sons, Inc., Hoboken, NJ, USA. pp. 294.

Kurokawa, K., Nakao, A., Wakabayashi, S., Fujimura, S., Eguchi, T., Matsunami, H., Yanai, J., 2020. Advanced approach for screening soil with a low radiocesium transfer to brown rice in Fukushima based on exchangeable and nonexchangeable potassium. *Sci. Total Environ.* 743. DOI: 10.1016/j.scitotenv.2020.140458.

Langmuir, D., 1997. *Aqueous Environmental Geochemistry*. Prentice Hall, Upper Saddle River, NJ, USA. pp. 600.

Larionova, N.V., Panitskiy, A.V., Kunduzbayeva, A.Y., Kabdyrakova, A.M., Ivanova, A.R., Aidarkhanov, A.O., 2021. Nature of radioactive contamination in soils of the pine forest in the territory adjacent to Semipalatinsk test site. *International Journal of Radiation Research* 19, 113-120. DOI: 10.18869/acadpub.ijrr.19.1.113.

Lutzenkirchen, J., Abdelmonem, A., Weerasooriya, R., Heberling, F., Metz, V., Marsac, R., 2014. Adsorption of dissolved aluminum on sapphire-c and kaolinite: implications for points of zero charge of clay minerals. *Geochemical Transactions* 15. DOI: 10.1186/1467-4866-15-9.

Lyklema, J., 1995. *Fundamentals of Interface and Colloid Science. Volume. II: Solid-Liquid Interfaces*. Academic Press, London, UK.

Marcus, Y., 1985. Ion Solvation. Wiley, Chichester, UK. pp. 306.

Matsunaga, T., Ueno, T., Amano, H., Tkatchenko, Y., Kovalyov, A., Watanabe, M., Onuma, Y., 1998. Characteristics of Chernobyl-derived radionuclides in particulate form in surface waters in the exclusion zone around the Chernobyl Nuclear Power Plant. *J. Contam. Hydrol.* 35, 101-113. DOI: 10.1016/s0169-7722(98)00119-3.

Mishra, S., Sahoo, S.K., Bossew, P., Sorimachi, A., Tokonami, S., 2016. Vertical migration of radio-caesium derived from the Fukushima Dai-ichi Nuclear Power Plant accident in undisturbed soils of grassland and forest. *J. Geochem. Explor.* 169, 163-186. DOI: 10.1016/j.gexplo.2016.07.023.

Missana, T., Garcia-Gutierrez, M., Alonso, U., 2008. Sorption of strontium onto illite/smectite mixed clays. *Phys. Chem. Earth* 33, S156-S162. DOI: 10.1016/j.pce.2008.10.020.

Missana, T., García-Gutiérrez, M., Benedicto, A., Ayora, C., De-Pourcq, K., 2014. Modelling of Cs sorption in natural mixed-clays and the effects of ion competition. *Appl. Geochem.* 49, 95-102. DOI: 10.1016/j.apgeochem.2014.06.011.

Motellier, S., Ly, J., Gorgeon, L., Charles, Y., Hainos, D., Meier, P., Page, J., 2003. Modelling of the ion-exchange properties and indirect determination of the interstitial water composition of an argillaceous rock. Application to the Callovo-Oxfordian low-water-content formation. *Appl. Geochem.* 18, 1517-1530.

Nie, Z., Finck, N., Heberling, F., Pruessmann, T., Liu, C., Lützenkirchen, J., 2017. Adsorption of selenium and strontium on goethite: EXAFS study and surface complexation modeling of the ternary systems. *Environ. Sci. Technol.* 51, 3751-3758. DOI: 10.1021/acs.est.6b06104.

Ning, Z.G., Ishiguro, M., Koopal, L.K., Sato, T., Kashiwagi, J., 2017. Strontium adsorption and penetration in kaolinite at low Sr²⁺ concentration. *Soil Sci. Plant Nutr.* 63, 14-17. DOI: 10.1080/00380768.2016.1277435.

Nordén, M., Ephraim, J.H., Allard, B., 1994. The influence of a fulvic acid on the adsorption of europium and strontium by alumina and quartz: effects of pH and ionic strength. *Radiochim. Acta* 65, 265-270. DOI: 10.1524/ract.1994.65.4.265.

Parkhurst, D.L., Appelo, C.A.J., 1999, User's Guide to PHREEQC (Version 2) — A Computer Program for Speciation, Batch-Reaction, One-Dimensional Transport, and Inverse Geochemical Calculations, U.S. Geological Survey, Water-Resources Investigations, Lakewood, Colorado, USA. Report 99-4259.

http://wwwbrr.cr.usgs.gov/projects/GWC_coupled/phreeqi/.

Parkhurst, D.L., Appelo, C.A.J., 2013, Description of Input and Examples for PHREEQC Version 3 — A Computer Program for Speciation, Batch-Reaction, One-Dimensional Transport, and Inverse Geochemical Calculations. Chapter 43 of Section A, Groundwater Book 6, Modeling Techniques, U.S. Geological Survey, Denver, Colorado, USA. p. 497.

<http://pubs.usgs.gov/tm/06/a43/pdf/tm6-A43.pdf>.

Peynet, V., 2003. Rétention d'Actinide et de Produits de Fission par des Phases Solides Polyminérales. PhD Thesis. Université Pierre et Marie Curie (Paris VI), Paris, France. pp. 273. In French.

Poinssot, C., Baeyens, B., Bradbury, M.H., 1999a. Experimental and modelling studies of caesium sorption on illite. *Geochim. Cosmochim. Acta* 63, 3217-3227. DOI: 10.1016/s0016-7037(99)00246-x.

Poinssot, C., Baeyens, B., Bradbury, M.H., 1999b, Experimental studies of Cs, Sr, Ni and Eu sorption on Na-illite and the modelling of Cs sorption, PSI, Villigen, Switzerland. Report NTB 99-04. p. 75.

http://www.nagra.ch/data/documents/database/dokumente/%24default/Default%20Folder/Publikationen/NTBs%201994-2000/e_ntb99-04.pdf.

Rafferty, P., Shiao, S.Y., Binz, C.M., Meyers, R.E., 1981. Adsorption of Sr(II) on clay minerals: effects of salt concentration, loading, and pH. *J. Inorg. Nucl. Chem.* 43, 797-805. DOI: 10.1016/0022-1902(81)80224-2.

Reiller, P.E., Descostes, M., 2020. Development and application of the thermodynamic database PRODATA dedicated to the monitoring of mining activities from exploration to remediation. *Chemosphere*. DOI: 10.1016/j.chemosphere.2020.126301.

Reinoso-Maset, E., Ly, J., 2014. Study of major ions sorption equilibria to characterize the ion exchange properties of kaolinite. *J. Chem. Eng. Data* 59, 4000-4009. DOI: 10.1021/je5005438.

Reynolds, R.C., 1985. Description of program NEWMOD for the calculation of the one-dimensional X-ray diffraction patterns of mixed-layered clays, Hanover, NH, USA. pp. 24.

Righi, D., Petit, S., Bouchet, A., 1993. Characterization of hydroxy-interlayered vermiculite and illite/smectite interstratified minerals from the weathering of chlorite in a cryorthod. *Clays Clay Miner.* 41, 484-495. DOI: 10.1346/Ccmn.1993.0410409.

Sahoo, S.K., Kavasi, N., Sorimachi, A., Arae, H., Tokonami, S., Mietelski, J.W., Łokas, E., Yoshida, S., 2016. Strontium-90 activity concentration in soil samples from the exclusion zone of the Fukushima daiichi nuclear power plant. *Sci. Rep.* 6, 23925. DOI: 10.1038/srep23925.

Samadfam, M., Jintoku, T., Sato, S., Ohashi, H., 2000. Effect of humic acid on the sorption of Sr(II) on kaolinite. *J. Nucl. Sci. Technol.* 37, 180-185. DOI: 10.1080/18811248.2000.9714882.

Savoye, S., Beaucaire, C., Fayette, A., Herbette, M., Coelho, D., 2012. Mobility of cesium through the Callovo-Oxfordian claystones under partially saturated conditions. *Environ. Sci. Technol.* 46, 2633-2641. DOI: 10.1021/Es2037433.

Savoye, S., Beaucaire, C., Grenut, B., Fayette, A., 2015. Impact of the solution ionic strength on strontium diffusion through the Callovo-Oxfordian clayrocks: an experimental and modeling study. *Appl. Geochem.* 61, 41-52. DOI: 10.1016/j.apgeochem.2015.05.011.

Sawhney, B.L., 1970. Potassium and cesium ion selectivity in relation to clay mineral structure. *Clays Clay Miner.* 18, 47-52. DOI: 10.1346/ccmn.1970.0180106.

Sawhney, B.L., 1972. Selective sorption and fixation of cations by clay minerals: a review. *Clays Clay Miner.* 20, 93-100. DOI: 10.1346/ccmn.1972.0200208.

Semenkova, A.S., Evsiunina, M.V., Verma, P.K., Mohapatra, P.K., Petrov, V.G., Seregina, I.F., Bolshov, M.A., Krupskaya, V.V., Romanchuk, A.Y., Kalmykov, S.N., 2018. Cs⁺ sorption onto Kutch clays: influence of competing ions. *Appl. Clay Sci.* 166, 88-93. DOI: 10.1016/j.clay.2018.09.010.

Siroux, B., Beaucaire, C., Benedetti, M.F., Reiller, P.E., 2017a. Adsorption of strontium and caesium onto an Na-MX80 bentonite: experiments and building of a coherent thermodynamic modelling. *Appl. Geochem.* 87, 167-175. DOI: 10.1016/j.apgeochem.2017.10.022.

Siroux, B., Beaucaire, C., Tabarant, M., Benedetti, M.F., Reiller, P.E., 2017b. Adsorption of strontium and caesium onto an Na-MX80 bentonite: experiments and building of a coherent thermodynamic modelling. *Appl. Geochem.* 87, 167-175. DOI: 10.1016/j.apgeochem.2017.10.022.

Siroux, B., Wissocq, A., Beaucaire, C., Latrille, C., Petcut, C., Calvaire, J., Tabarant, M., Benedetti, M.F., Reiller, P.E., 2018. Adsorption of caesium and strontium onto an Na-illite and Na-illite/Na-smectite mixtures: application of a multi-site ion-exchanger model. *Appl. Geochem.* 99, 65-74. DOI: 10.1016/j.apgeochem.2018.10.024.

Snyder, D.C., Delmore, J.E., Tranter, T., Mann, N.R., Abbott, M.L., Olson, J.E., 2012. Radioactive cesium isotope ratios as a tool for determining dispersal and re-dispersal mechanisms downwind from the Nevada Nuclear Security Site. *J. Environ. Radioact.* 110, 46-52. DOI: 10.1016/j.jenvrad.2012.01.019.

Stammose, D., Ly, J., Pitsch, H., Dolo, J.-M., 1992. Sorption mechanisms of three actinides on a clayey mineral. *Appl. Clay Sci.* 7, 225-238. DOI: 10.1016/0169-1317(92)90041-K.

Staunton, S., Dumat, C., Zsolnay, A., 2002. Possible role of organic matter in radiocaesium adsorption in soils. *J. Environ. Radioact.* 58, 163-173. DOI: 10.1016/S0265-931x(01)00064-9.

Steinhauser, G., Brandl, A., Johnson, T.E., 2014. Comparison of the Chernobyl and Fukushima nuclear accidents: A review of the environmental impacts. *Sci. Total Environ.* 470, 800-817. DOI: 10.1016/j.scitotenv.2013.10.029.

Tanaka, K., Takahashi, Y., Sakaguchi, A., Umeo, M., Hayakawa, S., Tanida, H., Saito, T., Kanai, Y., 2012. Vertical profiles of Iodine-131 and Cesium-137 in soils in Fukushima Prefecture related to the Fukushima Daiichi Nuclear Power Station accident. *Geochem. J.* 46, 73-76.

Tashiro, Y., Nakao, A., Wagai, R., Yanai, J., Kosaki, T., 2018. Inhibition of radiocesium adsorption on 2:1 clay minerals under acidic soil environment: effect of organic matter vs. hydroxy aluminum polymer. *Geoderma* 319, 52-60. DOI: 10.1016/j.geoderma.2017.12.039.

Tertre, E., Beaucaire, C., Coreau, N., Juery, A., 2009. Modelling Zn(II) sorption onto clayey sediments using a multi-site ion-exchange model. *Appl. Geochem.* 24, 1852-1861. DOI: 10.1016/j.apgeochem.2009.06.006.

Tournassat, C., Gailhanou, H., Crouzet, C., Braibant, G., Gautier, A., Gaucher, E.C., 2009. Cation exchange selectivity coefficient values on smectite and mixed-layer illite/smectite minerals. *Soil Sci. Soc. Am. J.* 73, 928-942. DOI: 10.2136/sssaj2008.0285.

Tournassat, C., Tinnacher, R.M., Grangeon, S., Davis, J.A., 2018. Modeling uranium(VI) adsorption onto montmorillonite under varying carbonate concentrations: A surface complexation model accounting for the spillover effect on surface potential. *Geochim. Cosmochim. Acta* 220, 291-308. DOI: 10.1016/j.gca.2017.09.049.

Villalobos, M., Leckie, J.O., 2000. Carbonate adsorption on goethite under closed and open CO₂ conditions. *Geochim. Cosmochim. Acta* 64, 3787-3802.

Wissocq, A., Beaucaire, C., Latrille, C., 2018. Application of the multi-site ion exchanger model to the sorption of Sr and Cs on natural clayey sandstone. *Appl. Geochem.* 93, 167-177. DOI: 10.1016/j.apgeochem.2017.12.010.

Yang, J.W., Jiang, X., Xu, R.K., Ji, G.L., Zhao, Q.G., 2003. Influence of ionic strength and lead concentrations on the adsorption of aluminum by a latosol. *Communications in Soil Science and Plant Analysis* 34, 2529-2537. DOI: 10.1081/css-120024784.

Yong, R.N., Nakano, M., Pusch, R., 2012. *Environmental Soil Properties and Behaviour*. CRC Press, Boca Raton, FL, USA.

Zaunbrecher, L.K., Cygan, R.T., Elliott, W.C., 2015. Molecular models of cesium and rubidium adsorption on weathered micaceous minerals. *J. Phys. Chem. A* 119, 5691-5700. DOI: 10.1021/jp512824k.

Zavarin, M., Roberts, S.K., Hakem, N., Sawvel, A.M., Kersting, A.B., 2005. Eu(III), Sm(III), Np(V), Pu(V), and Pu(IV) sorption to calcite. *Radiochim. Acta* 93, 93-102. DOI: 10.1524/ract.93.2.93.59413.